Bio-Optical Modeling of Primary Production on Regional Scales: The Bermuda BioOptics Project

D.A. Siegel[1*], T.K. Westberry[1], M.C. O'Brien[1], N.B. Nelson[2], A.F. Michaels[3], J.R. Morrison[2,4], A. Scott[2], E.A. Caporelli[3], J.C. Sorensen[1], S. Maritorena[1], S.A. Garver[5], E.A. Brody[1], J. Ubante[1] & M.A. Hammer[3]

1- Institute for Computational Earth System Science, University of California, Santa Barbara, Santa Barbara, CA 93106-3060, USA

2-Bermuda Biological Station for Research, Ferry Reach, GE-01, Bermuda

3-Wrigley Institute for Environmental Studies, University of Southern California, Los Angeles, CA 90089-0371, USA

4-Woods Hole Oceanographic Institution, Woods Hole MA 02543, USA

5-Department of Geography and Anthropology, California State Polytechnic University, Pomona, Pomona, CA 91768, USA

Submitted to *Deep-Sea Research Part II*, special issue on the BATS/HOT Time Series, October 15, 1999.

Resubmitted: February 9, 2000

KEYWORDS: primary production, regional models, bio-optical modeling, BATS, Sargasso Sea

[*] Corresponding author. Phone: (805) 893-4547 Fax: (805) 893-2578 Email: davey@icess.ucsb.edu

ABSTRACT:

Regional to global scale estimates of primary production must rely on remotely sensed quantities. Here, we characterize in situ light-primary production relationships and assess the predictive capability of several global primary production models using a 6-year time series collected as part of the U.S. JGOFS Bermuda Atlantic Time Series (BATS). The consistency and longevity of this data set provides an excellent opportunity to evaluate bio-optical modeling methodologies and their predictive capabilities for estimating rates of water column integrated primary production, $\int PP$, for use with satellite ocean color observations. We find that existing and regionally tuned parameterizations for vertically integrated chlorophyll content and euphotic zone depth do not explain much of the observed variability at this site. Fortunately, the use of these parameterizations for light availability and harvesting capacity has little influence upon modeled rates of $\int PP$. Site-specific and previously published global models of primary production both perform poorly and account for less than 40% of the variance in $\int PP$. A sensitivity analysis is performed to demonstrate the importance of light saturated rates of primary production, P^*_{sat}, compared with other photophysiological parameters. This is because nearly one-half of $\int PP$ occurs under light-saturated conditions. Unfortunately, we were unable to derive a simple parameterization for P^*_{sat} that significantly improves prediction of $\int PP$. The failure of global $\int PP$ models to encapsulate a major portion of the observed variance is due in part to the restricted range of $\int PP$ observations for this site. A similar result is found comparing global chlorophyll-reflectance algorithms to the present observations. More importantly, we demonstrate that there exists a time-scale (roughly 200 days) above which the modeled distributions of $\int PP$ are consistent with the observational data. By low-pass filtering the observed and modeled $\int PP$ time series, the model's predictive skill levels increase substantially. We believe that the assumptions of steady state and balanced growth used in bio-optical models of $\int PP$ are inconsistent with observational data. Most of the observed variance in $\int PP$ is driven by a variety of ecosystem disturbance processes that are simply not accounted for in bio-optical models. This puts important bounds on how $\int PP$ models should be developed, validated and applied.

I. INTRODUCTION:

Primary production, the conversion of dissolved inorganic carbon to particulate organic carbon through the utilization of absorbed light by phytoplankton, is a logical starting point for describing the marine carbon cycle. As the open ocean represents ~90% of the total ocean area (e.g., Ryther, 1969), it must be well understood if we are to understand the cycling of carbon on a global scale. The expanse of the ocean requires remote sensing techniques to be used to monitor changes in biogeochemical cycles, which in turn is limited by how well we can interpret the water leaving radiance spectrum. Further, the characterization and prediction of primary production rates from space require a determination of the ambient light field and its variability. The achievement of these goals provides the focus for the Bermuda BioOptics Project, or BBOP. BBOP has been making regular, profile observations of bio-optical parameters in conjunction with the U.S. JGOFS Bermuda Atlantic Time series Study (BATS) since January 1992. This is, to the best of our knowledge, the longest running time series of its kind for any oceanic region.

The Sargasso Sea off Bermuda is a unique environment as it may be characterized by both eutrophic and oligotrophic conditions during different times of the year (e.g., Menzel and Ryther, 1960; Michaels and Knap, 1996; Siegel et al., 1995a). This provides bio-optical data covering a reasonable dynamic range of possible conditions. This region has been observed nearly continuously since 1954 and is among the best characterized ocean sites on the planet (e.g., Michaels and Knap, 1996; Steinberg et al., 1999, this volume). Hydrostation S lies 25 km southeast of Bermuda and the 45+ year time-series record of biweekly hydrographic sampling is continuing at this station. The BATS site is 75 km southeast of Bermuda (31° 50' N; 64° 10' W). Since October 1988, BATS personnel have conducted nearly 150 cruises. Other time series observations are conducted off Bermuda, including determinations of deep sediment trap fluxes (Deuser, 1986; Conte et al., 1999, this volume), aerosol chemistry and deposition (e.g., Michaels et al., 1993) and an interdisciplinary moored science program (since 1994, the Bermuda

Testbed Mooring; Dickey et al., 1998). Clearly, BBOP builds on a long tradition of time-series research off the island of Bermuda.

As the Bermuda BioOptics Project is tightly linked with the BATS observational program, its scientific goals compliment the overall BATS efforts in many ways. Specifically, the scientific goals of the BBOP are to:

- characterize optical property variation; temporally, spatially and spectrally,
- assess light availability and its utilization within the marine food web,
- model primary production rates using optical quantities, and
- provide an "optical link" between BATS and satellite ocean color observations.

The accomplishment of these goals puts requirements on the nature of the sampling program. For instance, the goal of providing an optical link between BATS in situ observations and satellite ocean color imagery requires that mid-day observations of water-leaving radiance be determined during the BATS cruises. The accurate assessment of light availability and utilization rates requires that the BBOP optical observations match the time and location of the BATS in situ primary production array incubations.

In this contribution, we will use the BBOP and BATS data sets to assess and evaluate bio-optical models of primary production for clear ocean waters. The BBOP data set is perfect for these purposes as it is a multi-year time series (here 6 years) where consistent methodologies have been applied. Hence, differences will not arise due to changes in protocols for primary production rate determinations, phytoplankton pigment concentrations or radiometric calibration. The primary objective here is to develop and validate relationships with which satellite data can be used to estimate primary production. Each element in the bio-optical modeling approach is assessed. This includes the estimation of surface chlorophyll from in situ reflectance spectra and the determination of the vertically integrated chlorophyll content, depth of euphotic zone and details of the chlorophyll profile from a measure of surface chlorophyll. A hierarchy of primary production models is compared with the BATS/BBOP data set in order to

develop an understanding of the primary regulating factors and to quantify the predictive capabilities of bio-optical models. The results of these data-model evaluations are disappointing and reasons for these poor evaluations are discussed. In particular, we demonstrate that the present data-model assessment for primary production rates is an "apples vs. oranges comparison" due to the very nature of the models and observational data sets. Finally, these results are used to suggest bounds of applicability for the bio-optical approach to modeling primary production rates.

II. DATA AND METHODS:

The Bermuda Bio-Optics Program (BBOP) began collecting data in January 1992 in conjunction with the on-going U.S. JGOFS Bermuda Atlantic Time-series Study (BATS). The BATS station is located nominally at 31° 50' N, 64° 10' W within the oligotrophic waters of the Sargasso Sea. There are typically 16 cruises per year, conducted monthly with additional cruises during the spring bloom period, January through May. Primary production, pigments and nutrients were measured once during each cruise. Primary production arrays were incubated at 8 depths between 0 and 140 m from sunrise to sunset using the light-dark ^{14}C method. Rates of vertically integrated primary production, $\int PP$, are determined by integrating the primary production profile over the upper 140 m of the water column. Pigment samples (4 liters) were drawn from a near noon-time cast at 12 depths in the upper 250 m, filtered onto 2.5 cm GF/F filters and analyzed using high-pressure liquid chromatography (HPLC, Bidigare et al., 1989; Knap et al., 1993). Values of upper ocean chlorophyll content, $\int Chl$, are determined by integrating the vertical chlorophyll *a* concentration profile with respect to depth over the upper 140 m. Nutrient samples (nitrate+nitrate, phosphate and silicic acid) were collected from 10 to 12 depths in the upper 200 m and analyzed by standard colorometric techniques (Knap et al., 1993). Additional details about the BATS primary production, pigment and nutrient analyses are available (cf., Lohrenz et al., 1992; Knap et al., 1993; Michaels et al., 1994; Siegel et al., 1995a; Michaels and Knap, 1996; Steinberg et al., 1999, this volume; Sorensen and Siegel, 1999, this volume).

Continuous profiles of in situ optics were collected in the upper 200 m using a profiling spectroradiometer (MER-2040, Biospherical Instruments Inc., San Diego CA; Smith et al., 1984; 1996). The primary optical measurements are downwelling vector irradiance and upwelling radiance, $E_d(z,\lambda,t)$ and $L_u(z,\lambda,t)$, respectively. During 1992 and 1993, these were measured in eight downwelling (410-665 nm) and nine upwelling (410-683) wavebands. Since January 1994, the instrument has sampled 12 wavebands for downwelling irradiance and upwelling radiance (410, 441, 465, 488, 510, 520, 555, 565, 589, 625, 665 and 683 nm). The BBOP sampling package also includes temperature and conductivity (SeaBird, Bellevue WA), chlorophyll fluorescence and red beam transmission (SeaTech, Corvallis OR) sensors. Incident downwelling vector irradiance, $E_d(0^+,\lambda,t)$, was measured using a second mast-mounted spectroradiometer with wavebands similar to the underwater instrument. Data products include profiles of diffuse attenuation coefficients for downwelling irradiance and nadir upwelling radiance ($K_d(z,\lambda,t)$, $K_L(z,\lambda,t)$) calculated over a 10 m depth window and remote sensing reflectance ($R_{rs}(0^-,\lambda,t) = L_u(0^-,\lambda,t)/E_d(0^-,\lambda,t)$). Analysis procedures are documented in Siegel et al. (1995b). The spectroradiometers are calibrated three times per year at UCSB and calibration uncertainties are of order of 1% (O'Brien et al., 1999). Several other bio-optical measurements are made as part of the BBOP program but are not used in the present analyses. These include in situ vertical profiles of spectral absorption and beam attenuation coefficients using a WET Labs AC-9 (Brody, 1998) and discrete determinations of particulate, phytoplankton and dissolved absorption spectra (e.g., Nelson et al., 1998).

The BBOP radiometer deployments are optimized to match-up with the BATS primary production observations. During the primary production incubations, radiometer casts are conducted every two hours, weather permitting. Nearly 20 BBOP profiles are available for each primary production determination (Table 1). Typically, 14 primary production profiles are taken each year where BBOP radiometry is adequate for estimating daily light doses. The near-continuous daily record of $E_d(0^+,\lambda,t')$ is used to estimate daily mean averages of the flux of photosynthetically available radiation (PAR). Observations

of incident irradiance spectrum are integrated over the visible spectrum (400-700 nm), and daylight hours, or

$$PAR(0^+,t) = \int_{400}^{700} \int_{SR}^{SS} \frac{\lambda}{hc} E_d(0^+,\lambda,t')\,dt'\,d\lambda \qquad (1)$$

where t is year day, t' is time resolved through a diel cycle and the factor λ/hc accounts for conversion of an energy flux to a quantum flux. Determinations of the in situ PAR flux, $PAR(z,t)$, are made using a cruise mean spectral transmittance profile, $TR(z,\lambda,t)$, or

$$PAR(z,t) = \int_{400}^{700} \frac{\lambda}{hc}(1-r)\,TR(z,\lambda,t) \int_{SR}^{SS} E_d(0^+,\lambda,t')\,dt\,d\lambda \qquad (2a)$$

where r accounts for the transmission of irradiance across the sea surface (=0.02; e.g., Mobley, 1994) and values of $TR(z,\lambda,t)$ are defined as

$$TR(z,\lambda,t) = \frac{1}{N_{pro}} \sum_{n=1}^{N_{pro}} \frac{E_d(z,\lambda,t_n)}{E_d(0^+,\lambda,t_n)} \qquad (2b)$$

where N_{pro} are the number of profiles used to define $TR(z,\lambda,t)$ for a given day. Typically, irradiance profiles are taken 3 hours of each side of local noon resulting in about 7 profiles used for each $TR(z,\lambda,t)$ determination. The clear-sky PAR flux, $PAR_{CS}(0^+,t)$, is calculated using the radiative transfer model of Ricchiazzi et al. (1998) assuming a standard mid-latitude summer atmosphere with oceanic boundary layer aerosols.

The BBOP/BATS light-productivity data set analyzed here is provided in the CD-ROM that comes with this volume or via the World Wide Web (`ftp://ftp.icess.ucsb.edu/pub/bbop/ProdData/`). Data are provided by cruise and by individual bottle basis (filenames = CD_data_surf.dat and CD_data_z.dat, respectively). Documentation is provided in the respective README files.

III. Annual and Interannual Variations in the BioOptical Fields

The time-depth distributions of in situ temperature, nitrate nutrient concentration and mixed layer depth (MLD) show the expected seasonal cycles off Bermuda (Figures 1a and 1c). Winter-time deep mixing brings elevated nutrient concentrations into the surface waters providing the new nutrients required to support the annual spring bloom (e.g., Menzel and Ryther, 1960; 1961; Siegel et al., 1990; 1995a; 1999; Michaels et al., 1994; Doney et al., 1996). The process of winter-time convective transport of nutrients is clearly seen in the time-depth distributions of temperature, nitrate concentration and the depths of the mixed layer and the nitracline. Restratification in early spring essentially stops the convective inputs of nutrient rich waters to the surface resulting in a spring bloom as predicted by Sverdrup's (1953) spring bloom hypothesis. The spring bloom is manifest in the time-depth changes of primary production rates (Figure 1d). During the summer, the temperature of the mixed layer approaches 30 C and a robust seasonal cycle in temperature is observed throughout the upper 120 m (Figure 1a). Summer-time mixed layer depths are rarely less than 25 m. The salinity distribution (Figure 1b) also shows a significant seasonal cycle as the near-surface waters freshen during the summer and become more saline during periods of deep mixing. This is driven to a large degree by seasonal changes in the evaporative losses (e.g., Warren, 1972; Doney, 1996). Deep mixing occurs again in the fall and the seasonal cycle repeats itself.

The time-depth distribution of primary production shows the expected pattern of high values in the late-winter and early-spring as part of the spring bloom and lower rates throughout the rest of the year (Figure 1d). Most of the primary production occurs within the upper 75 m or so of the water column and a subsurface production maximum is rarely observed. The extent and duration of elevated primary production appears to be related to the strength and persistence of the winter mixing conditions. Maximum carbon assimilation rates are nearly 25 mgC m^{-3} d^{-1} in the near-surface layers while typical summer-time values are roughly 4 mgC m^{-3} d^{-1}.

The spring bloom is also evident in the distributions of the chlorophyll *a* concentration and estimates of $K_d(z,490,t)$ (Figures 2a and 2b). Elevated near-surface concentrations of chlorophyll *a* occur coincidentally with the deep mixing observed in the late-winter and the elevated primary production rates. Peak near-surface chlorophyll *a* concentrations are ~0.4 mg m^{-3} during the spring bloom. During the summer, surface chlorophyll *a* concentrations are reduced (typically 0.05 mg m^{-3}) and a subsurface chlorophyll maximum is observed roughly coincident with the depths of 1% PAR isolume and the nitracline. A significant fall bloom of phytoplankton is observed only in the fall seasons of 1992 and 1994. The same general patterns are found in $K_d(z,490,t)$ although there is considerably more noise in its determination from a spectral irradiance profile (Figure 2b; e.g., Siegel et al., 1995a). The depth of the euphotic zone is defined operationally using the depth of the 1% PAR isolume, $Z_{1\%PAR}$ which has a mean value of 91 meters and a standard deviation of 13 meters (N=82). Values of $Z_{1\%PAR}$ do not show a strong seasonal variation but are subject to short-time scale variations coincident with changes in position of the chlorophyll *a* maximum (Figure 2a). Changes in the depth of the chlorophyll *a* concentration maximum and the 1% PAR isolume followed closely the depth of the nitracline (Figures 1 and 2). The depths of all three isosurfaces changed consistently with the presence of anomalous thermohaline water masses. This evidence suggests that subsurface nutrient and PAR fluxes have roles in the formation or maintenance of the subsurface chlorophyll *a* maximum (e.g., Siegel et al., 1990; 1995a; Doney, 1996; McGillicuddy et al., 1998; 1999).

The ratio of $K_d(z,410,t)$ to $K_d(z,490,t)$ has been shown to be a reliable index for non-algal absorption at this site (Siegel and Michaels, 1996; Garver and Siegel, 1997). Discrete absorption measurements have shown this signal to be dominated by changes in the concentration of colored dissolved organic materials or CDOM (Nelson et al., 1998). The annual cycle of the $K_d(z,410,t)$ to $K_d(z,490,t)$ ratio is similar throughout the entire BBOP record as that discussed for 1992 and 1993 by Siegel and Michaels (1996). The dynamics of CDOM have been hypothesized to be due to bacterial production at depth and loss from photo-oxidation in the summer mixed layer (Nelson et al., 1998; in

preparation). Winter-time mixing homogenizes CDOM concentrations throughout the water column and the annual cycle repeats itself.

The time-wavelength distribution of the remote-sensing reflectance, $R_{rs}(0^-,\lambda,t)$, quantifies the color of the ocean and provides the link to ocean color satellites (e.g., Gordon and Morel, 1983; Garver and Siegel, 1997; O'Reilly et al., 1998). The ocean is obviously "bluer" in the summer when the $R_{rs}(0^-,\lambda,t)$ spectrum peaks towards the violet and "greener" in the winter and spring periods where the $R_{rs}(0^-,\lambda,t)$ spectrum is much less peaked. These spectral shape differences are the basis for ocean color algorithms (e.g., Gordon and Morel, 1983).

Significant interannual changes are apparent in the 6 year BBOP-BATS time series. For example, convective mixing was relatively strong during the winters of 1992, 1995 and 1996 creating deep sustained mixed layers (>200m) while the winter mixed layer depths for 1993 and 1994 were shallower and shorter in duration (Figure 1). This suggests that winter convective inputs of new nutrients will have significant interannual changes which appear to be in agreement with the intensity and duration of the spring blooms observed in primary production rates and chlorophyll *a* concentrations. In addition, the salinity distribution provides a useful measure of water mass variability at this site (e.g., Siegel et al., 1995a; Doney, 1996). During the spring of 1997, extremely high salinity values (≥ 37 psu) indicated that the BATS site was affected by non-local water masses.

Of particular interest is the large subsurface maximum in primary production observed in July of 1995 (Figure 1d). This event resulted in the highest chlorophyll *a* concentrations observed at BATS (Figure 2a; Chl ≥ 1 mg m^{-3}). This event was sampled by autonomous nutrient and pigment sensors on the Bermuda Testbed Mooring (McNeil et al., 1999). This event corresponded to the presence of an 18° water eddy which had uplifted nutrient-replete waters into the euphotic zone while deflecting downward the main thermocline. Many other mesoscale eddy events have been observed at BATS

which have a significant influence on regional biogeochemical processes (Siegel et al., 1995a; 1999; Doney, 1996; McGillicuddy et al., 1998; 1999; McNeil et al., 1999).

IV. Bio-Optical Modeling of Pigment Biomass & In Situ Light

A primary purpose of this manuscript is to test methods for assessing rates of primary production from satellite ocean color data and to evaluate the utility of these algorithms for studying change in global marine productivity. Most bio-optical models of primary production require estimates of phytoplankton pigment biomass and PAR. Hence, we will assess the reliability of predicting near-surface chlorophyll *a* concentrations from a measure of ocean color, $R_{rs}(0^-,\lambda,t)$, of estimating the water column burden of chlorophyll pigment, $\int Chl$, and the vertical profile of chlorophyll, $Chl(z)$ from a measure of surface chlorophyll, $Chl(0)$, and of determining the PAR flux at depth from a measure of $Chl(0)$. In each we compare to global algorithms which have been proposed by previous investigators and when appropriate provide a regional update to these algorithms. This is important as most bio-optical parameterizations have been derived using global data sets where chlorophyll concentrations range over three orders of magnitude (e.g., Gordon and Morel, 1983; Smith and Baker, 1978; Morel, 1988; 1991; Morel and Berthon, 1989; Balch et al., 1992; Balch and Bryne, 1994; O'Reilly et al., 1998). The BBOP/BATS data set has a much smaller range of chlorophyll concentrations. For example at BATS, $Chl(0)$ values are always less than 0.5 mg m^{-3} and nearly one-half (47%) of them are less than 0.1 mg m^{-3}. This enables us to test regional specificity of these global parameterizations and to tune them for specific regional conditions.

The chlorophyll *a* algorithm selected for SeaWiFS satellite mission was derived using global data set of remote sensing reflectance and chlorophyll estimates, the SeaBAM data set (O'Reilly et al., 1998). An updated version of this algorithm, OC2v2 (Maritorena and O'Reilly, 1999), applied to the BBOP data set shows that the algorithm explains 61% of the variability in the BATS HPLC chlorophyll *a* determinations (large open circles in Figure 3a). For comparison purposes, all of the SeaBAM data with chlorophyll *a*

concentrations less than 0.35 mg m^{-3} are included as the dots in Figure 3a. The OC2v2 algorithm explains 64% of this subset of the SeaBAM data set. The predictive capability of the OC2v2 algorithm for the BBOP data set is about the same as that for the SeaBAM data set when evaluated over the similar ranges of chlorophyll concentrations. However, BBOP data set makes up 23% of the SeaBAM data set for *Chl*(0) concentrations less than 0.35 mg m^{-3}. Hence, this is not an independent test of the OC2v2 algorithm. Regardless, the predictive skill of the OC2v2 algorithm is much greater when assessed over the entire SeaBAM data set (r^2 = 91%). The issue of regional vs. global tuning of empirical algorithms will be addressed further in the discussion.

Several simple models for $\int PP$ require estimation of the total chlorophyll content in the euphotic zone, $\int Chl$. It is also used to determine the mean chlorophyll concentration of the euphotic zone assuming a uniform distribution ($Chl_{Uni}(z,t) = \int Chl(t)/140$ m). Values of $\int Chl$ increase with *Chl*(0) as expected although a large amount of scatter is observed (Figure 3b). The power law formulation of Morel and Berthon (1989) severely underestimates the $\int Chl$ observations and all of the relationships explain about 50% (Table 2a). Root mean square deviations are smallest for the locally tuned relations with values of ~6 mg m^{-2}.

The depth of the 1% PAR isolume, $Z_{1\%PAR}$, is also typically required for modeling $\int PP$. As expected, values of $Z_{1\%PAR}$ decrease with *Chl*(0) (Figure 3c). Established relationships (Smith and Baker, 1978; Morel, 1988; Balch et al., 1992), as well as regionally tuned fits, all perform poorly (Table 2b). This poor predictive capability (r^2 ~ 30%) is due in part to the relatively small amount of variance in $Z_{1\%PAR}$ (s.d. = 12.6 m).

The vertical profile of the chlorophyll *a* concentration is often modeled using a Gaussian profile (e.g., Lewis et al., 1983; Morel and Berthon, 1989; Morel, 1991; Sathyendranath et al., 1995; Longhurst et al., 1995). This enables the subsurface maximum in phytoplankton pigment biomass to be accounted for in the modeling of productivity. In addition, the Gaussian fit parameters have been used to delineate different "biogeochemical provinces" for driving primary production models (e.g., Platt

and Sathyendranath, 1988; Longhurst et al., 1995; Longhurst, 1998). The fit parameters for the Gaussian chlorophyll profile can also be parameterized using a measurement of $Chl(0)$ (e.g., Morel and Berthon, 1989; Morel, 1991). This enables the entire chlorophyll profile to be determined using only an estimate of $Chl(0)$. Following Morel and Berthon (1989), the Gaussian chlorophyll concentration profile, $Chl_{Gauss}(z)$, is modeled as

$$Chl_{Gauss}(z) = Chl_{Uni}(z)\left[C_b + \left(C_{\max} - C_b\right)\exp\left(-\left(\frac{z - z_{\max}}{\Delta z}\right)^2\right)\right] \qquad (3)$$

where z is the physical depth, z_{max} is the depth of the subsurface chlorophyll maximum, Δz is the thickness of the chlorophyll maximum and, $C_b(t)$ and $C_{max}(t)$ are scaling factors for the background and peak chlorophyll concentrations, respectively. The parameters z_{max} and Δz are actually fit using optical depth ($\zeta = K_{par}\, z$) and are denoted as ζ_{max} and $\Delta\zeta$, respectively. The Gaussian profile parameters, $\Delta\zeta$, ζ_{max}, C_b and C_{max} are fit for each profile using a non-linear least squares procedure (Press et al., 1990). For most of the profiles, the Gaussian model did a good job predicting more than 70% of the variance in an individual profile. However, some poor fits (less than 50% variance explained) occurred for 14 out of the 78 total number of days (18% of the total). These failures occurred for a variety of factors and these data were not used in the final parameterization.

The distribution of the $Chl_{Gauss}(z)$ fit parameters as a function of $Chl(0)$ is shown in Figure 4. In general, only a weak correspondence between the individual fit parameters and $Chl(0)$ is found (Table 3). Using the parameterizations provided in Table 3, the BBOP-tuned Gaussian model predicts the observed chlorophyll profile considerably better than the Morel and Berthon (1989) global parameterization although just one-half of the total variance is explained (Table 4). Both of the Gaussian models evaluated out perform the uniform profile model, $Chl_{Uni}(z)$. Further, both the BBOP-tuned Gaussian model and the Morel and Berthon (1989) global parameterization do a fair job of predicting temporal variations in upper ocean chlorophyll pigment content, $\int Chl$, (Table

2a). However, the predictive understanding is not much better than the simple, empirical linear or power-law relationships.

Accurate estimates of the $PAR(z,t)$ flux are also required for most bio-optical models of primary production. Simple estimates of the $PAR(z,t)$ can be made by assuming that the transmission profile for PAR, $TR(z,PAR,t)$ described entirely by the depth of the 1% PAR isolume, or

$$TR(z,PAR,t) = \exp(- \ln(0.01)\, z / Z_{1\%PAR}) \qquad (4a)$$

and the PAR flux at depth, $PAR(z,t)$ can be expressed as

$$PAR(z,t) = (1-r)\, PAR(0^{+},t)\, TR(z,PAR,t) \qquad (4b)$$

where r is the sea surface transmission of irradiance (r = 0.02). Hence from a measure of surface chlorophyll and incident light, estimates of $PAR(z,t)$ can be determined. All of the models evaluated here work well (explaining more than 90% of the variability) in predicting $PAR(z,t)$ and $TR(z,PAR,t)$ (Table 5). Both comparisons are presented to eliminate any spurious positive correlation arising from changes in $PAR(0^{+},t)$. Estimates made using the locally tuned $Z_{1\%PAR}$ relationship work better than global algorithms, but not to a highly significant degree. Interestingly, estimates of $PAR(z,t)$ and $TR(z,PAR,t)$ using the mean observed value of $Z_{1\%PAR}$ explain a surprisingly large degree of the variability in the directly measured quantities. This means that the three order of magnitude variation in $TR(z,PAR,t)$ with depth (Equation 4a) has a much greater impact on modeled values of $TR(z,PAR,t)$ than do temporal variations in the value of $Z_{1\%PAR}$. Hence, the bio-optical modeling of $PAR(z,t)$ is not highly dependent upon a detailed knowledge of the depth of the 1% PAR isolume for this site.

V. LIGHT-PRIMARY PRODUCTION RELATIONSHIPS AT BATS

Time-series of incident light, chlorophyll content and integrated primary production

Time series observations of incident PAR, $PAR(0^+,t)$, vertically integrated chlorophyll *a* content, $\int Chl(t)$, and integrated primary production, $\int PP(t)$, are shown in Figure 5. To a large extent, the time course of $PAR(0^+,t)$ follows that for the clear sky atmosphere although large deviations associated with the sampling of cloudy days are found. Mean value of the atmospheric transmission ($=PAR(0^+,t)/PAR_{CS}(0^+,t)$) at BATS is about 70% (Table 6) which is greater than the value of 50% (4 okta) assumed in the modeling study of Fasham et al. (1990) for this same region.

The time course of integrated chlorophyll content and integrated primary production show the expected seasonal patterns with higher values observed in the spring periods of each year (Figure 5). A large degree of interannual variability is also seen as years 1992, 1995 and 1996 have intense spring blooms (peak $\int PP > 1000$ mgC m^{-2} d^{-1}) whereas years 1994 and 1997 have small spring blooms (peak $\int PP < 700$ mgC m^{-2} d^{-1}). Similar, though not exact, patterns are seen in the integrated chlorophyll content. These differences in intensity are likely to be driven by interannual changes in convective nutrient inputs (e.g., Menzel and Ryther, 1961; Siegel et al., 1990; 1995a; 1999; Michaels et al., 1994; Doney et al., 1996). The ensemble mean value of $\int PP$ is 460 mgC m^{-2} d^{-1} which is much greater than the seminal observations of Menzel and Ryther (1961) (which is roughly 100 mgC m^{-2} d^{-1}). This huge difference is due to improvements in primary production methodologies with the advent of trace metal clean techniques (e.g., Fitzwater et al., 1982; Michaels and Knap, 1996; Sorensen and Siegel, 1999, this volume). There is also great deal of variability about the values of $\int PP$ and $\int Chl$ as estimates of the coefficient of variation (C.V. = standard deviation / mean) are 50.6 and 37.5%, respectively.

Ψ-Based Modeling of $\int PP$

The relationship between light, upper ocean chlorophyll content and water column integrated primary production can be expressed in terms of the photosynthetic light

utilization index, Ψ (e.g., Falkowski, 1981; Platt, 1986). Values of Ψ are a measure of the time-integrated rate of carbon fixation per unit area, normalized by $\int Chl$ and time-integrated photon flux (units of mgC m^2 $mgChl^{-1}$ E^{-1}). Estimates of $\Psi(t)$ are defined using

$$\int PP(t) = \Psi(t) \int Chl(t)\, PAR(0^+,t) \qquad (5)$$

The single term, $\Psi(t)$, encapsulates changes in important physiological and biophysical parameters such as the in situ quantum yield for carbon fixation, and the chlorophyll-specific phytoplankton absorption coefficient. It has been proposed that Ψ is relatively constant on regional scales and perhaps globally, hence it may be considered a biogeochemical constant (e.g., Platt, 1986; Morel, 1991). As the components of Ψ exhibit significant variability according to several environmental parameters (e.g., Kishino et al., 1986; Sorensen and Siegel, 1999, this volume) it would be expected that Ψ be highly variable as well (e.g., Campbell and O'Reilly, 1988; Cullen, 1990; Siegel et al., 1995a).

Values of Ψ range from 0.16 to nearly 3 mgC m^2 $mgChl^{-1}$ E^{-1} (Figure 5). The mean for the period 1992-1997 (N=82) is 0.75 mgC m^2 $mgChl^{-1}$ E^{-1} (Table 6) which is lower than our previous report using a subset of the present dataset ($\langle\Psi\rangle$ = 0.92 mgC m^2 $mgChl^{-1}$ E^{-1}, N=29, years 1992 and 1993 only; Siegel et al., 1995a). However, this value is still much larger than the globally-fixed value which has been proposed to model global primary productivity (0.44 mgC m^2 $mgChl^{-1}$ E^{-1}; Platt, 1986; Morel and Berthon, 1989). Estimates of Ψ are also characterized by a high degree of variability (C.V. = 49%) which suggests that using a constant Ψ to model production in the area will fail to capture a majority of the variance in primary production measurements. Similar to Siegel et al. (1995a), there appeared to be no apparent seasonal signal in Ψ estimates and only weak inverse relationships were found between determinations of Ψ and $\int Chl$ (r^2=0.10) and between Ψ and $PAR(0^+)$ (r^2=0.12).

As expected, the Ψ-based approach (Equation 5) for predicting ∫PP explains only 27% of its variability when the ensemble mean Ψ estimate is used (Table 7). No real improvements are observed if values of Ψ are empirically modeled using the surface chlorophyll concentration and/or the incident PAR flux (Table 7). Further, when the chlorophyll content, $\int Chl$, is modeled using the surface chlorophyll, $Chl(0)$, (Table 2a), the predictive skill does not significantly change. Thus, Ψ-based approaches to the modeling of $\int PP$ predict less than ~30% of the variance in $\int PP$ even when tuned to a given site. This indicates that more information about the factors regulating $PP(z)$ is required.

Assessing the Light-Production Relationship and its Role in Predicting ∫PP

As is well recognized, rates of primary production are, to first order, a function of the in situ photon flux. This simple relationship constitutes the predictive basis of nearly every primary production model/algorithm (e.g, Bidigare et al., 1992; Behrenfeld and Falkowski, 1997b). A useful method for characterizing the primary production observations is by assessing their relationship with the in situ light field using a hyperbolic tangent production-irradiance model (e.g., Jassby and Platt, 1976), or

$$PP^*(z,t) \equiv PP(z,t)/Chl(z,t) = P^*_{sat}(t) \tanh\left[PAR(z,t)/I_k(t)\right] \qquad (6)$$

where $PP^*(z,t)$ is the assimilation number (units of mgC mgChl^{-1} d^{-1}), $P^*_{sat}(t)$ is the saturated rate of chlorophyll-normalized production (mgC mgChl^{-1} d^{-1}), and $I_k(t)$ is the light intensity at which saturation occurs (E m^{-2} d^{-1}). This formulation treats the water column as a compound photosynthetic system (Talling, 1957), in contrast to a standard photosynthesis versus irradiance experiment where a single water sample is incubated at several different light levels. Hence, differences among the parameters derived from the two approaches should be expected. This analysis provides parameters that are useful for diagnosing the role of light saturation on observations of primary production. Estimates of $P^*_{sat}(t)$ and $I_k(t)$ are retrieved from the BATS/BBOP data set using a non-linear least-

squares analyses based upon the Levenberg-Marquardt algorithm (Press et al., 1990; Siegel et al., 1995a).

Values of $P^*_{sat}(t)$ range from 10 to greater than 300 mgC mgChl^{-1} d^{-1} and do not show an obvious seasonal cycle (Figure 5). On the other hand, retrievals of $I_k(t)$ have a seasonal cycle with an amplitude of ~10 E m^{-2} d^{-1}where the maximum occurs in the spring. Overall, values of $I_k(t)$ range from nearly 0 to over 20 E m^{-2} d^{-1}. The observed range of P^*_{sat} and I_k retrievals are typical for this site compared with standard P-I determinations (e.g., Lohrenz et al., 1992). Ensemble mean values for $P^*_{sat}(t)$ and $I_k(t)$, $<P^*_{sat}>$ and $<I_k>$, are 75.6 (43.1 s.d.) mgC mgChl^{-1} d^{-1} and 5.42 (4.47 s.d.) E m^{-2} d^{-1}, respectively (Table 6).

The retrievals of $I_k(t)$ can be compared with determinations of the daily mean, in situ PAR flux to determine the light level and depth where light limitation occurs (e.g., Siegel et al., 1995a). Mean values of $I_k(t)/PAR(0^+,t)$ are ~18% which corresponds to a mean physical depth of 37 m (Table 6). A time course of the depth of where the in situ PAR flux is equal to the retrieved value of $I_k(t)$ (defined here as Z_{Ik}) is shown in Figure 2d. About one-half of the total amount of primary production occurs above Z_{Ik} (Table 6) indicating the importance of modeling the saturated rates of primary production.

The hyperbolic tangent light-primary production relationship (Equation 6) is an excellent interpolator for describing compactly the $PP(z)$ profile. That is, predictions of $PP(z)$ and $\int PP$ using daily specified values of $P^*_{sat}(t)$ and $I_k(t)$ predict 80 and 82% of the variance, respectively (Table 8). However when ensemble mean values of P^*_{sat} and I_k are applied, only 53 and 19% of the variance is predicted for $PP(z)$ and $\int PP$, respectively. These results are consistent with Siegel et al.'s (1995a) analysis of the 1992-1993 BATS/BBOP data set. The relative importance of P^*_{sat} and I_k can be assessed by allowing one of these parameters to vary as a function of time while the other remains fixed (Table 8). Hindcast skills for $PP(z)$ and $\int PP$ are significantly greater when P^*_{sat} is allowed to vary in time and I_k is fixed (75 and 65% of the variance for $PP(z)$ and $\int PP$, respectively) compared with the case for which P^*_{sat} is fixed and I_k is permitted to vary

(53 and 19% for PP(z) and $\int PP$, respectively). This experiment again demonstrates the importance of correct estimates of light saturated rates of primary production.

The present framework for modeling $PP(z)$ and $\int PP$ can also be used to assess the importance of modeling the chlorophyll concentration, using either an uniform profile, $Chl_{Uni}(z,t)$, or a Gaussian profile, $Chl_{Gauss}(z,t)$, and for the PAR profiles, using a linear relationship. As expected, the modeled chlorophyll profiles did not perform as well as the observed values although $Chl_{Gauss}(z,t)$ clearly out performed $Chl_{Uni}(z,t)$ (Table 8). For cases where the ensemble mean value of P^*_{sat} is used, there is little loss of predictive skill as the predictions with the observed $Chl(z,t)$ profile are poor to start with. However, the uniform chlorophyll profile performs poorly when the mean I_k is used and P^*_{sat} is taken as a function of time (Table 8). The modeling of $PAR(z,t)$ has a small effect on the prediction of $\int PP$ although skill levels for $PP(z)$ are typically reduced. This is likely the effect that the errors in modeling $PAR(z,t)$ accumulate deeper into the water column and they subsequently influence the modeling of $PP(z)$ at depth much more than the modeling of $\int PP$.

In an attempt to improve the empirical predictions of $\int PP$, monthly mean values of P^*_{sat} and I_k are used in the estimation of $PP(z)$ and $\int PP$. Using either the observed or modeled $Chl(z,t)$ and $PAR(z,t)$ profiles, only marginal improvements were found compared with the cases where ensemble mean values of P^*_{sat} and I_k are used (Table 8). Values of P^*_{sat} and I_k were also empirically modeled using a stepwise, multiple linear regression technique (e.g., Davis, 1977; Siegel and Dickey, 1986). Empirical correlates included sea surface temperature, daily integrated PAR, daylength, fraction of clear sky PAR, and $Chl(0)$. Unfortunately, very weak statistical relationships were found. The best predictor was the surface chlorophyll concentration which explained 15 and 11% of the variance in P^*_{sat} and I_k, respectively, or

$$\hat{P}^*_{sat} = -176\ Chl(0) + 91 \qquad (7a)$$

$$\hat{I}_k = -18.8\ Chl(0) + 7.3 \qquad (7b)$$

More complicated parameterizations were attempted; however the artificial skill introduced by increasing input parameters exceeded the increase in overall prediction skill (cf., Siegel and Dickey, 1986). Again, application of these simple parameterizations did not improve significantly predictions of $PP(z)$ or $\int PP$ (Table 8). These analyses show that simple, empirical models of $PP(z)$ and $\int PP$ seem to be limited in their predictive capability.

A Test of Several Global Primary Production Models using the BATS Data Set:

A major goal of international satellite ocean color programs is to estimate globally the distribution of primary production from satellite (e.g., Platt et al., 1995). To accomplish this, a plethora of models and algorithms have been developed (e.g., Ryther and Yentsch, 1957; Balch et al., 1992; Bidigare et al., 1987; 1992; Cullen, 1990; Behrenfeld and Falkowski, 1997a; 1997b; Morel, 1991; Antoine and Morel, 1996; Platt and Sathyendranath, 1988; Platt et al., 1991; 1995; Sathyendranath et al., 1989; 1995; Longhurst et al., 1995; Campbell et al., in preparation). These approaches all assume the existence of an analytical relationship between $\int PP$ or $PP(z)$ and measures of incident PAR flux and surface chlorophyll. Here, we compare the predictions made by several global $\int$PP models using the BATS/BBOP data set. The goal of these comparisons is not to show which of the models "works the best", but rather to demonstrate the degree to which these models explain temporal variability and can be used to understand and monitor temporal changes of the global marine biosphere.

A common ancestor for most $\int PP$ models is the algorithm introduced by Ryther and Yentsch (1957) (hereafter RY57). This model assumes that $\int PP$ can be modeled as a simple function of the incident light field and chlorophyll or

$$\int PP = \frac{4.8\, Chl(0)\, Z_{1\%\, PAR}}{4.605}\left(1 - e^{-0.0528\ \mathrm{PAR}(0^+)}\right) \qquad (8)$$

where Cullen's (1990) parameterizations for the RY57 model are used. The RY57 model does a poor job predicting the observed mean $\int PP$ (underestimates by 46%) or the

observed variability (r^2 = 34%; Table 7). This underestimate is interesting considering that Menzel and Ryther (1961) used the RY57 model as an index of *gross* primary production in comparison with their carbon assimilation measurements off Bermuda. Menzel and Ryther (1961) found that annual rates of primary production (determined using ^{14}C incubations) were about a factor of 50% less than the RY57 gross productivity estimate. The RY57 model now severely underestimates BATS $\int PP$ observations suggesting that important methodological changes (i.e., trace metal clean collection and incubation, improved filter technology, isotope stock purity, etc.) have occurred in the forty-plus intervening years.

Recently, Behrenfeld and Falkowski (1997a; hereafter BF97) introduced a reduced, vertically generalized production model to predict daily, depth-integrated water column production within the euphotic zone using

$$\int PP = 0.661\ P^*_{opt}\ \frac{PAR(0^+)}{PAR(0^+)+4.1}\ Z_{1\%\,PAR}\ C_{opt}\ D_{irr} \qquad (9)$$

where P^*_{opt} is the maximum assimilation rate within the water column, C_{opt} is the chlorophyll concentration at the depth where P^*_{opt} is found and D_{irr} is daylength. For BATS, values of P^*_{opt} will equal P^*_{sat} as photoinhibition is rarely observed in $PP(z)$ profiles (see Figure 1d). This also means that C_{opt} is equivalent to $Chl(0)$. The BF97 model parameterizes P^*_{opt} in terms of surface temperature using a 7th order polynomial and it assumes that the details of the pigment biomass profile are unimportant. Results with the BF97 model are not much better than the RY57 model as only 20% of the variance the individual $\int PP$ determinations is explained (Table 7). Using individual determinations of P^*_{sat} for each profile, 73% of the variance in $\int PP$ is predicted within the BF97 framework (Equation 8). This further amplifies the importance of knowing the saturated rate of primary production for predicting $\int PP$.

The model of Platt et al. (1995) represents the culmination of many studies by the authors and their colleagues. The model is based upon a fixed relationship between photosynthetic rates and light for a given location or province. The model can be run in

two modes; the first uses a constant biomass profile and analytically solves the equations of Platt et al. (1990), the second numerically integrates the spectral equations presented in Sathyendranath et al. (1989) with modifications as described by Sathyendranath et al. (1995). In both cases, mean seasonal and regional photosynthesis parameters are taken from Sathyendranath et al. (1995) and Platt et al. (1991). The model code was taken from the World Wide Web (`http://www.ioccg.org/software/Ocean_Production/index.html`; Platt and Sathyendranath, 1999). Predictions of $\int PP$ with the Platt/Sathyendranath model are again rather poor, as only about 20% of the variance in $\int PP$ is explained (Table 7). In addition, both implementations of the model result in severe underestimates of the mean conditions (by 50%). There are little differences observed whether a uniform chlorophyll distribution or a Gaussian profile for chlorophyll biomass is used.

The Waters/Bidigare model, as used in Ondrusek et al. (1999, this volume), estimates volume rates of primary production as the product of an effective quantum yield, Φ_c, multiplied by the quantum flux of PAR absorbed by phytoplankton. Estimates of Φ_c are parameterized as a function of irradiance following Bidigare et al. (1992) using data taken directly from the Sargasso Sea (Waters et al., 1994). Phytoplankton absorption coefficients, $a_{ph}(\lambda)$, as well as many other photophysiological parameters may be calculated using a suite of possibilities provided in the model code. Code and documentation are available at `http://satftp.soest.hawaii.edu/piglet/prod_model/index.html`. Various combinations of physiological parameters, inherent optical property and subsurface biomass distributions were applied following the options in the model. The final and best performing combination used mean maximum quantum yields for this site (Sorensen and Siegel, 1999, this volume), the Bricaud et al. (1995) $a_{ph}(\lambda)$ parameterizations and specifications of the biomass profile using the BBOP Gaussian $Chl(z,t)$ model. This combination of parameters performed the best of all the models used as 41% of the variance in $\int$PP is explained by this "tuned" version of this model.

Antoine and Morel (1996) offer a Ψ-based model, where the value of Ψ is derived from a bio-optical model of production (Morel, 1991). Values of Ψ are assumed to be a function of day of year, latitude, fraction of cloudiness, surface chlorophyll, and sea surface temperature. The Antoine and Morel (1996) model is applied in the form of a look-up table for two cases: 1) a vertically homogenous chlorophyll distribution and 2) a stratified water column. As was seen with all of the previous ∫PP models, the two formulations of the Antoine and Morel (1996) model do not compare well with the in situ data records as 22 to 27% of the variance in ∫PP is explained (Table 7). No significant differences are found whether the water column is uniform or stratified in the estimation of Ψ as parameterized by Antoine and Morel (1996).

The various modeled and observed ∫PP time series are shown in Figure 6. Results from the ∫PP models are not differentiated in Figure 6 as there are few real distinguishing characteristics among them. The different model results appear to envelope the data set quite reasonably; however, the size of the "envelope" of model results is quite large (on the average 414 mgC m^{-2} d^{-1}). Further, the collection of models appears to capture many of the nuances of the long-time scale trends quite reasonably although the point-to-point differences are quite poor. The mean of the 9 global ∫*PP* models presented in Table 7 is debatably the best performer of all the models evaluated, predicting 39% of the variance in ∫PP with a normalized mean bias of 11% (Table 7).

VI. Discussion

It should be apparent that the various bio-optical models of water column integrated primary production did not perform well as predictors of the observed ∫PP time series. This includes models designed to predict global distributions of primary production and their change in time as well as models empirically tuned to the BATS data set. These problems cannot be attributed simply to data quality issues as the sampling and analysis methodologies have been consistently applied over the six-year record (see Sorensen and Siegel, 1999, this volume). Further, the present results are not due to peculiarities of this

site as other investigators have experienced similar difficulties in modeling ∫PP. These comparisons have used global data sets (e.g., Balch et al., 1992; Campbell et al., in preparation) as well as regional ones including the U.S. JGOFS Hawaii Ocean Time series station (Letelier et al., 1996; Ondrusek et al., 1999, this volume), the northeastern U.S. coastal zone (Campbell and O'Reilly, 1988), the southeastern U.S. continental shelf (e.g., Yoder et al., 1985), Antarctic coastal waters (Claustre et al., 1997), the tropical Pacific Ocean (Banse and Yong, 1990) and the California current (e.g., Cullen, 1990; Balch et al., 1992). Hence, we believe that the observed poor performance of the bio-optical approach is a fundamental issue. In the following, we show that this is due to the nature of primary production observations and the assumptions used in developing bio-optical models.

Empirical Modeling on Regional Scales

The poor performance of the ∫*PP* models begs the question "Do these models really work this bad when applied globally?" A part of the reason for the poor predictive skill observed is the relatively small dynamic range in the BATS ∫*PP* time series compared with global observations of ∫*PP*. For example, the data set used by BF97 to derive empirically their ∫*PP* model has 3.4 times the variance as the BATS ∫*PP* time series (Figure 7). Hence, there is a larger dynamic range to develop empirical models. The BF97 model explains 56% of the variance in ∫*PP* when applied to the global data set used to develop it (Figure 7). This global estimate of r^2 for the BF97 model is not that much greater the best r^2 determinations (~40%) from the BATS/BBOP data set (Table 7). We can sub-sample the BF97 data set by choosing model-data pairs that are consistent with the BATS chlorophyll observations. One realization of this random sampling is shown as the insert in upper-left corner of Figure 7. Overall, the BF97 model explains very little of any random realization of the BF97 subset and on the average only 17% of the variance in the modeled ∫*PP* is explained using this "BF97-lite" data set (ensemble mean NMB = -38%). This reestablishes our intuition that empirical modeling building requires a significant variance range over which we can statistically explain variability.

Previously we showed that the global chlorophyll algorithm used by the SeaWiFS project in its operational processing (OC2v2) performs only adequately for the BATS time series (Figure 3a). For this data set, the OC2v2 algorithm explains only 61% of the observed variance in *Chl*(0); whereas over the entire global SeaBAM data set, the OC2v2 algorithm explains 91% of the variance in the near-surface chlorophyll. Correspondingly low predictive skills were found using the OC2v2 algorithm for a low chlorophyll subset of the SeaBAM data set ("SeaBAM-lite ??"). The present regional validation of the OC2v2 chlorophyll algorithm is exactly analogous to that found using the "BF97-lite" version of the BF97 $\int PP$ global data set.

In a sense, empirical models attempt to explain natural phenomena by attempting to account for the primary regulating processes. For example, most $\int$PP models assume that the incorporation of carbon by phytoplankton is balanced by the absorption of light and assimilation of nutrients as modified by light saturation and temperature dependent processes. These simple models are tuned against data using a cost function as an objective measure of success. However, the assumed regulating processes must be well represented in the data set. As analytical representations of interacting marine biological processes are poor at best, only the first order processes will be accounted for. Hence, the greatest empirical modeling successes will be found using data sets that extend over as large of a range of possible marine ecosystems. Hence, empirical $\int$PP models enjoy reasonable success when evaluated over globally distributed data (Figure 7).

Another way to look at this is to consider the distribution of observations by biome and ecological regime (R. Letelier, personal communication, 1999). The present results indicate that empirical models seem to work reasonably well when evaluated across several biomes, but rather poorly when evaluated within a single biome. Empirical models parameterize reasonably well the large scale, first order processes that regulate the temporal changes in productivity across biomes. However, these models do not appear to perform well within a biome. It seems likely that many, second-order "disturbance" processes help regulate changes in $\int$PP within a biome. These processes

may include episodic inputs of macro- and micro-nutrients, day-to-day changes in solar illumination and/or vertical mixing, mesoscale eddy-induced changes in water mass and/or light climate, predator-prey cycles within the grazer community, etc. (e.g., Goldman, 1993; Michaels et al., 1993; Siegel, 1998; McGillicuddy et al., 1998; Siegel et al., 1995a; 1999; Sorensen and Siegel, 1999, this volume). As variability in the first order regulating processes will be relatively small within an open ocean biome, the influence of these complex, disturbance processes is likely to be more important to regulating temporal changes in $\int PP$. It seems doubtful that improvements in $\int PP$ models will occur until a predictive understanding of the effects of ecosystem disturbance on rates of $\int PP$ is developed.

They're only models, right?

This brings us to the question of whether the nature of the models themselves has any bearing on their poor validation. As referred to previously, models of $\int PP$ assume relationships among the absorption and utilization of light energy, the assimilation of inorganic carbon and nutrients, the production of biomass and the role of temperature. Built into these models are the important assumptions of steady state and balanced growth (Cullen, 1990). In short, these assumptions allow one to predict dynamics ($\int PP$) from determinations of stock abundance (*Chl*) as modified by exogenous factors (PAR and temperature). These assumptions have been very successful for predicting *steady state* rates of primary production in laboratory culture experiments (e.g., Laws and Bannister, 1980; Kiefer and Mitchell, 1983; Sakshaug et al., 1989). However, it seems unlikely that planktonic ecosystems will be at steady state and balanced, especially for open ocean sites where ecosystem disturbances appear to be the rule rather than the exception.

The balanced growth assumption can begin to be tested using the BATS $\int PP$ time series. We assert that ecosystem disturbance processes are regulating the dominant fraction of $\int PP$ variability and that these processes may be characterized by time scales of a month or less. Once the quasi-random noise signal due to ecosystem disturbance is

removed, one would expect a much higher degree of fidelity between the bio-optical model results and observations. Evidence of a short time scale for disturbance can be found in short decorrelation time scales, $\tau_{\int PP}$, observed for the BATS $\int PP$ time series (29.6 days; Sorensen and Siegel, 1999, this volume). Estimates of $\tau_{\int PP}$ quantify the scale over which each observation is statistically independent from the previous one and are calculated as the integral of the time-lagged autocorrelation function to the first zero crossing (e.g., Davis, 1977; Bendat and Piersol, 1986). The present determination of $\tau_{\int PP}$ (29.6 days) is nearly identical to the mean time between BATS cruises (26.4 days) indicating that each BATS cruise is basically an independent observation (e.g., Siegel et al., 1995a; Doney, 1996).

Importantly, the short decorrelation time scale for ∫PP suggests that ecosystem disturbances are first order episodic and random relative to the BATS sampling schedule. Hence, we expect to find reasonable correspondence between the model and observed time series for long time scales and significantly reduced correlation levels for shorter time scales. Determinations of coherence spectra are a convenient means for addressing the role of time scale in the comparison of two time series (e.g., Bendat and Piersol, 1986; Emery and Thomson, 1997). Estimates of spectral coherence between the observed $\int PP$ time series and the nine ∫PP models presented in Table 7 are shown as the solid lines in Figure 8. The periods resolved in this analysis range from 500 to 42 days. Again, the nine $\int PP$ models are not differentiated in this analysis, as the behavior among them is similar. Statistically significant correspondence (at the 90% confidence level) is found between the observed and modeled time series only for the time scales greater than 200 days (Figure 8).

Spectral analyses performed on rather short, oddly sampled time series are often problematic (e.g., Bendat and Piersol, 1986; Emery and Thomson, 1997). We examined the effects of BATS sampling schedule and random noise on the coherence estimates using a pair of sinusoids with periods of 300 and 400 days (the dashed lines in Figure 8). Each time series is sampled following the BATS schedule and Gaussian random noise

with variance equal to the signal's variance is added to one of the pairs. As expected, significant coherence is found only at the appropriate frequencies (Figure 8). However, this test supports the present calculation of a coherence time scale from the BATS data set.

To illustrate the importance of the coherence time scale, we created high-passed and low-passed time series and compared the correlation coefficients between the model-data pairs (Table 9). A third order Butterworth filter and a time scale of 200 days was used to perform the digital filtering (following the Matlab® procedure, butter.m). Variability in Table 9 is quantified as the standard deviation in the low- and/or high-pass time series normalized by the unfiltered time series. As expected, the predictive skills between the low-pass filtered model-data pairs are often a factor of two larger than the sample r^2 estimate presented previously (Table 9). Although the maximum skill is only 56% of the low-pass time series variability of the observed $\int PP$ record, this value is identical to that found for the BF97 model against the global data set used to parameterize its form (Figure 7). Virtually no correspondence is observed between the high-pass filtered model-data pairs which are considerably worse than are found for the sampled time series (Table 9). There is roughly a factor of three less variability in the low-pass filtered time series than is found in the high-passed time series. Hence, predictive skill levels found using the low-pass time series are much higher although there is considerably less variance contained in this record.

The present filtering exercise supports the hypothesis that ecosystem disturbance mechanisms, which lead to unbalanced growth and a non-steady state ecosystem, are, to first order, episodic and random. This work also demonstrates that for this site the amplitude of the "disturbance" signal (high-pass variance signal in Table 9) is much greater than the amplitude of the "balanced growth" signal. Last, we show that the present model-data comparisons are valid only over proper time scales (> 200 days) which places a fundamental constraint on the application of the bio-optical approach to predicting $\int PP$ with satellite data.

Building, Applying and Validating Bio-Optical Models of Primary Production

The time scale analyses presented here point toward the steady-state and balanced growth assumptions as the major contributors to the poor predictive skill observed for $\int PP$ models. In essence, the validation of the present generation of $\int PP$ models using field observations can be thought of as an "apple vs. orange comparison". The models assume balanced growth whereas the field data are point observations of an inherently unsteady and unbalanced ecosystem. When model results and field observations are evaluated in a manner consistent with the assumptions in the models, the predictive success of the model increases substantially. The poor performance of the many global $\int PP$ models presented here does *not* mean that they should not be used for addressing global biogeochemical cycles. Rather, the present analyses provide a time scale over which their application is valid. For this site, this time scale is roughly 200 days. It seems reasonable that this result will be fundamental and will hold for other ocean regions.

The existence of a cutoff time scale for bio-optical model applicability raises the question of an analogous spatial scale above which the quasi-random unbalanced growth signal will be averaged out. Mechanisms of ecosystem disturbance occur on spatial scales ranging from centimeters to hundreds of kilometers. As many of the processes leading to episodic bursts of new nutrients are associated with interactions with mesoscale eddies or atmospheric deposition, it is likely that this scale should be at least several hundred kilometers. It is difficult to provide even an educated guess of how this cutoff scale interacts with the temporal scale addressed previously. However, it appears reasonable that the bio-optical approach will be valid over relatively large spatial scales (several 100 km) and long time scales (~200 days).

Last, the present results reveal that there are inherent limits to the use of randomly distributed observations to develop and validate bio-optical models of $\int PP$. This has been seen by other investigators validating models using global data sets (e.g., Balch et al., 1992; Campbell et al., in preparation). Clearly, improvements in the collection and construction of data used to develop and validate these models are needed. One obvious way would be to make determinations of primary production that are highly resolved data

in both time and space. Opportunities are available to make determinations of carbon assimilation rates at daily resolution from moored platforms (e.g., Taylor and Doherty, 1990). Similar approaches are required if we are to get beyond our present status of comparing apples and oranges.

Acknowledgements – The many contributors to BBOP would like to thank the scientists and technicians of the U.S. JGOFS BATS program for many good years of collaboration. We gratefully appreciate the hard work and dedication of the masters, crew and marine technicians of the R/V Weatherbird II. We also thank David Antoine, Mike Behrenfeld, John Cullen, Shubha Sathyendranath and Kirk Waters for help in implementing the bio-optical models presented. Barney Balch, Bob Bidigare, Mark Brzezinski, Scott Doney, Rod Johnson, Ricardo Letelier, Dennis McGillicuddy, Joel Michaelsen, Julie Siegel, Ray Smith and Libe Washburn have provided useful discussions and sometimes encouragement. Gus and Alida provided much needed distractions. BBOP is supported by NASA through the auspices of the SeaWiFS science team, the U.S. JGOFS synthesis and modeling and the SIMBIOS programs. BATS is supported by the NSF.

REFERENCES:

Antoine, D., Morel, A., 1996. Oceanic primary production, 1, Adaptation of a spectral light-photosynthesis model in view of application to satellite chlorophyll observations. Global Biogeochemical Cycles 10, 43-55.

Balch, W.M., Bryne, C.F., 1994. Factors affecting the estimate of primary production from space. Journal of Geophysical Research 99, 7555-7570.

Balch, W.M., Evans, R., Brown, J., Feldman, G., McClain, C., Esaias, W., 1992. The remote sensing of ocean primary productivity - the use of a new data compilation to test satellite algorithms. Journal of Geophysical Research 97, 2279-2293.

Banse, K., Yong, M., 1990. Sources of variability in satellite-derived estimates of phytoplankton production in the eastern tropical Pacific. Journal of Geophysical Research 95, 7201-7215.

Behrenfeld, M.J., Falkowski, P.G., 1997a. Photosynthetic rates derived from satellite-based chlorophyll concentration. Limnology and Oceanography 42, 1-20.

Behrenfeld, M.J., Falkowski, P.G., 1997b. A consumer's guide to phytoplankton primary production models. Limnology and Oceanography 42, 1479-1491.

Bendat, J.S., Piersol, A.G., 1986. Random Data. J. Wiley and Sons, New York.

Bidigare, R.R., Morrow, J.H., Kiefer, D.A., 1989. Derivative analysis of spectral absorption by phytoplankton pigments in the western Sargasso Sea. Journal of Marine Research 47, 323-341.

Bidigare, R.R., Prézelin, B.B., Smith, R. C., 1992. Bio-Optical Models and the Problems of Scaling. In: Falkowski, P.G., Woodhead, A.D. (Eds.), Primary Productivity and Biogeochemical Cycles in the Sea, Plenum Press, New York, pp. 175-212.

Bidigare, R.R., Smith, R.C., Baker, K.S., Marra, J., 1987. Oceanic primary production estimates from measurements of spectral irradiance and pigment concentrations. Global Biogeochemical Cycles 1, 171-186.

Bricaud, A., Babin, M., Morel, A., Claustre, H., 1995. Variability in the chlorophyll-specific absorption coefficients of natural phytoplankton: analysis and parameterization. Journal of Geophysical Research 100, 13321-13331.

Brody, E.A., 1998. Validation and modeling of in situ inherent optical properties in the Sargasso Sea. Master Thesis, Geography Department, University of California, Santa Barbara, Santa Barbara, California.

Campbell, J.W., and others, 1999. The SeaWiFS primary production intercomparison study. In preparation.

Campbell, J.W., O'Reilly, J.E., 1988. Role of satellites in estimating primary productivity on the northwest Atlantic continental shelf. Continental Shelf Research 8, 179-204.

Claustre, H., Moline, M.A., Prezelin, B.B., 1997. Sources of variability in the column photosynthetic cross section for Antarctic coastal waters. Journal of Geophysical Research 102, 25047-25060.

Conte, M.H., Ralph, N., Ross, E.H., 1999. Seasonal and interannual variability in deep ocean particle fluxes at the Oceanic Flux Program (OFP)/Bermuda Atlantic Time Series (BATS) site in the western Sargasso Sea near Bermuda. This volume.

Cullen, J.J., 1990. On models of growth and photosynthesis in phytoplankton, Deep-Sea Research 37, 667-683.

Davis, R.E., 1977. Techniques for statistical analysis and prediction of geophysical fluid systems. Geophysical and Astrophysical Fluid Dynamics 8, 245-277.

Deuser, W.G., 1986. Seasonal and interannual variations in deep-water particle fluxes in the Sargasso Sea and their relation to surface hydrography. Deep-Sea Research 33, 225-246.

Dickey, T., Frye, D., Jannasch, H., Boyle, E., Manov, D., Sigurdson, D., McNeil, J., Stramska, M., Michaels, T., Nelson, N., Siegel, D., Chang, G., Woo, J., 1998. Preliminary results from the Bermuda testbed mooring program. Deep-Sea Research Part I 45, 771-794.

Doney, S.C., 1996. A synoptic atmospheric surface forcing data set and physical upper ocean model for the US JGOFS Bermuda Atlantic Time-series Study site. Journal of Geophysical Research 101, 25615-25634.

Doney, S.C., Glover, D.M., Najjar, R.G., 1996. A new coupled, one-dimensional biological-physical model of the upper ocean: Applications to the JGOFS Bermuda-Atlantic Time-series Study (BATS) site. Deep-Sea Research Part II 43, 591-624.

Emery, W.J., Thomson, R.E., 1997. Data Analysis Methods in Physical Oceanography. Pergamon Press, New York.

Falkowski, P.G., 1981. Light-shade adaptation and assimilation numbers. Journal of Plankton Research 3, 203-216.

Fasham, M.J.R., Ducklow, G.W., McKelvic, S.M., 1990. A nitrogen-based model of plankton dynamics in the oceanic mixed layer. Journal of Marine Research 48, 591-639.

Fitzwater, S.E., Knauer, G.A., Martin, J.H., 1982. Metal contamination and its effects on primary production measurements. Limnology and Oceanography 27, 544-551.

Garver, S.A., Siegel, D.A., 1997. Inherent optical property inversion of ocean color spectra and its biogeochemical interpretation: I. Time series from the Sargasso Sea. Journal of Geophysical Research 102, 18607-18625.

Goldman, J.C., 1993. Potential role of large oceanic diatoms in new primary production. Deep-Sea Research Part I 40, 159-168.

Gordon, H.R., Morel, A.Y., 1983. Remote Assessment of Ocean Color for Interpretation of Satellite Visible Imagery: A Review. Spring-Verlag, New York.

Jassby, A.D., Platt, T., 1976. Mathematical formulation of the relationship between photosynthesis and light for phytoplankton. Limnology and Oceanography 21, 540-547.

Kiefer, D.A., Mitchell, B.G., 1983. A simple steady state description of phytoplankton growth based on absorption cross-section and quantum efficiency. Limnology and Oceanography 28, 770-776.

Kishino, M., Okami, N., Takahashi, M., Ichimura, S., 1986. Light utilization efficiency and the quantum yield of phytoplankton in a thermally stratified sea. Limnology and Oceanography 31, 557-566.

Knap, A.H., and others, 1993. BATS Methods - March 1993, BATS Method Manual Version 3. Woods Hole MA: U.S. JGOFS Planning and Coordination Office.

Laws, E.A., Bannister, T.T., 1980. Nutrient- and light-limited growth of Thalassiosira fluviatilis in continuous culture, with implications for phytoplankton growth in the ocean. Limnology and Oceanography 25, 457-473.

Letelier, R.M., Dore, J.E., Winn, C.D., Karl, D.M., 1996. Seasonal and interannual variations in photosynthetic carbon assimilation at Station ALOHA. Deep-Sea Research Part II 43, 467-490.

Lewis, M.R., Cullen, J.J., Platt, T., 1983. Phytoplankton and thermal structure in the upper ocean: Consequences of nonuniformity in chlorophyll profile. Journal of Geophysical Research 88, 2565-2570.

Lohrenz, S.E., Knauer, G.A., Asper, V.L., Tuel, M., Michaels, A.F., Knap, A.H., 1992. Seasonal and interannual variability in primary production and the particle flux in the northwestern Sargasso Sea: U.S. JGOFS Bermuda Atlantic Time series Station. Deep-Sea Research 39, 1373-1391.

Longhurst, A., 1998. Ecological Geography of the Sea. Academic Press, San Diego, CA.

Longhurst, A., Sathyendranath, S., Platt, T., Caverhill, C., 1995. An estimate of global primary production in the ocean from satellite radiometer data. Journal of Plankton Research 17, 1245-1271.

Maritorena, S., O'Reilly, J., 1999. Update on the operational SeaWiFS chlorophyll a algorithm. In: SeaWiFS Postlaunch Calibration and Validation Analyses, Part 2, SeaWiFS Postlaunch Technical Report Series, NASA Tech. Memo. 1999-206892, Vol. 9, Hooker, S.B., Firestone, E.R. (Eds.), NASA Goddard Space Flight Center, Greenbelt, Maryland. Accepted.

McGillicuddy Jr., D.J., Johnson, R.J., Siegel, D.A., Michaels, A.F., Bates, N., Knap, A.H., 1999. Mesoscale variability of ocean biogeochemistry in the Sargasso Sea. Journal of Geophysical Research 104, 13381-13394.

McGillicuddy Jr., D.J., Robinson, A.R., Siegel, D.A., Jannasch, H.W., Johnson, R., Dickey, T.D., McNeil, J., Michaels, A.F., Knap, A.H., 1998. Influence of mesoscale eddies on new production in the Sargasso Sea. Nature 394, 263-266.

McNeil, J.D., Jannasch, H.W., Dickey, T., McGillicuddy, D., Brzezinski, M.A., Sakamoto, C.M., 1999. New chemical, bio-optical and physical observations of upper ocean response to the passage of a mesoscale eddy off Bermuda. Submitted to Journal of Geophysical Research.

Menzel, D.W., Ryther, J.H., 1960. The annual cycle of primary production in the Sargasso Sea off Bermuda. Deep-Sea Research 6, 351-366.

Menzel, D.W., Ryther, J.H., 1961. Annual variations in primary production of the Sargasso Sea off Bermuda. Deep-Sea Research 7, 282-228.

Michaels, A.F, Siegel, D.A., Johnson, R., Knap, A.H., Galloway, J.N., 1993. Episodic inputs of atmospheric nitrogen to the Sargasso Sea: Contributions to new production and phytoplankton blooms. Global Biogeochemical Cycles 7, 339-351.

Michaels, A.F., Knap, A.H., 1996. Overview of the U.S. JGOFS Bermuda Atlantic Time-series Study and the Hydrostation S program. Deep-Sea Research Part II 43, 157-198.

Michaels, A.F., Knap, A.H., Dow, R.L., Gundersen, K., Johnson, R.J., Sorensen, J.C., Close, A., Knauer, G.A., Lohrenz, S.E., Asper, V.A., Tuel, M., Bidigare, R., 1994. Seasonal patterns of ocean biogeochemistry at the U.S. JGOFS Bermuda Atlantic Time-series Study site. Deep-Sea Research 41, 1013-1038.

Mobley, C.D., 1994. Light and Water; Radiative Transfer in Natural Waters, Academic Press, San Diego, CA.

Morel, A., 1988. Optical modeling of the upper ocean in relation to its biogenous matter content (case I waters). Journal of Geophysical Research 93, 10749-10768.

Morel, A., 1991. Light and marine photosynthesis: a spectral model with geochemical and climatological implications. Progress in Oceanography 26, 263-306.

Morel, A., Berthon, J.F., 1989. Surface pigments, algal biomass profiles, and potential production of the euphotic layer: Relationships reinvestigated in view of remote sensing applications. Limnology and Oceanography 34, 1545-1562.

Nelson, N.B., Siegel, D.A., Michaels, A.F., 1998. Seasonal dynamics of colored dissolved material in the Sargasso Sea. Deep-Sea Research Part I 45, 931-957.

O'Brien, M.C., Menzies, D.W., Siegel, D.A., Smith, R.C., 1999. Calibration history for the UCSB radiometers and ocean optics calibration laboratory. NASA Tech. Memo. In press.

Ondrusek, et al., 1999. Primary production modeling at Station Aloha. This volume. In press.

O'Reilly, J., Maritorena, S., Mitchell, B.G., Siegel, D.A., Carder, K.L., Kahru, M., Garver, S.A., McClain, C.R., 1998. Ocean color algorithms for SeaWiFS. Journal of Geophysical Research 103, 24937-24953.

Platt T, Sathyendranath, S., Longhurst, A., 1995. Remote sensing of primary production in the ocean - Promise and fulfillment. Philosophical Transactions of the Royal Society of London Series B: Biological Sciences 348, 191-201.

Platt, T., 1986. Primary production of the ocean water column as a function of surface light intensity, algorithms for remote sensing. Deep-Sea Research 33, 149-163.

Platt, T., Caverhill, C.M., Sathyendranath, S., 1991. Basin-scale estimates of oceanic primary production by remote sensing: The North Atlantic, Journal of Geophysical Research 96, 15147-15159.

Platt, T., Sathyendranath, S., 1988. Oceanic primary production: Estimation by remote sensing at local and regional scales. Science 241, 1613-1620.

Platt, T., Sathyendranath, S., 1999. Software for Use in Calculation of Primary Production in the Oceanic Water Column. WWW Page, http://www.ioccg.org/software/Ocean_Production/index.html.

Platt, T., Sathyendranath, S., White III, G.N., Ravindran, P., 1990. Primary production by phytoplankton: analytic solutions for daily rates per unit area of water surface, Proceedings of the Royal Society of London Series B 241, 101-111.

Press W.H., Tuekolsky, S.A., Vettering, W.T., Flannery, B.P., 1990. Numerical Recipes in C: The Art of Scientific Computing, Cambridge University Press.

Ricchiazzi, P.J., Yang, S., Gautier, C., 1998. SBDART: A research and teaching software tool for plane-parallel radiative transfer in the Earth's atmosphere, Bulletin of the American Meteorological Society 79, 2101-2114.

Ryther, J.H., 1969. Photosynthesis and fish production in the sea. Science 166, 269.

Ryther, J.H., Yentsch, C.S., 1957. The estimation of phytoplankton production form chlorophyll and light data. Limnology and Oceanography 2, 281-286.

Sakshaug, E., Andresen, K., Kiefer, D.A., 1989. A steady state description of growth and light absorption in the marine planktonic diatom Skeletonema costatum. Limnology and Oceanography 34, 198-205.

Sathyendranath, S., Longhurst, A., Caverhill, C.M., Platt, T., 1995. Regionally and seasonally differentiated primary production in the North Atlantic, Deep-Sea Research Part I 42, 1773-1802.

Sathyendranath, S., Platt, T., Caverhill, C.M., Warcock, R.E., Lewis, M.R., 1989. Remote sensing of oceanic primary production: computations using a spectral model. Deep-Sea Research 36, 431-453.

Siegel, D.A., 1998. Resource competition in a discrete environment: Why are plankton distributions paradoxical? Limnology and Oceanography 43, 1133-1146.

Siegel, D.A., Dickey, T.D., 1986. Variability of net longwave radiation over the eastern North Pacific Ocean. Journal of Geophysical Research 91, 7657-7666.

Siegel, D.A., Fields, E., McGillicuddy, Jr., D.J., 1999. Mesoscale motions, satellite altimetry and new production in the Sargasso Sea. Journal of Geophysical Research 104, 13359-13379.

Siegel, D.A., Iturriaga, R., Bidigare, R.R., Pak, H., Smith, R.C., Dickey, T.D., Marra, J., Baker, K.S., 1990. Meridional variations of the springtime phytoplankton community in the Sargasso Sea. Journal of Marine Research 48, 379-412.

Siegel, D.A., Michaels, A.F., 1996. Quantification of non-algal light attenuation in the Sargasso Sea: Implications for biogeochemistry and remote sensing. Deep-Sea Research Part II 43, 321-345.

Siegel, D.A., Michaels, A.F., Sorensen, J.C., O'Brien, M.C., Hammer, M., 1995a. Seasonal variability of light availability and its utilization in the Sargasso Sea. Journal of Geophysical Research 100, 8695-8713.

Siegel, D.A., O'Brien, M. C., Sorensen, J. C., Konnoff, D., Fields, E., 1995b. The BBOP Methods Manual. Woods Hole: U.S. JGOFS Planning Office.

Smith, R.C., Baker, K.S., 1978. Optical classification of natural waters. Limnology and Oceanography 23, 260-267.

Smith, R.C., Booth, C.R., Star, J.L., 1984. Oceanographic biooptical profiling system. Applied Optics 23, 2791-2797.

Smith, R.C., Menzies, D.W., Booth, C.R., 1996. Oceanographic bio-optical profiling system II. SPIE Ocean Optics XIII 2963, 777-789.

Sorensen, J.C., Siegel, D.A., 1999. Variability of the effective quantum yield for carbon assimilation in the Sargasso Sea. This volume.

Steinberg, D., Carlson, C.A., Bates, N.R., Johnson, R.J., Michaels, A.F., Knap, A.H., 1999. Overview of the US JGOFS Bermuda Atlantic Time-series Study (BATS): A decade-scale look at ocean biology and biogeochemistry. This volume.

Sverdrup, H.U., 1953. On the conditions for the vernal blooming of phytoplankton. Journal du Conseil, Conseil Permanent International pour l' Exploration de la Mer 18, 287-295.

Talling, J.F, 1957. The phytoplankton population as a compound photosynthetic system. New Phytologist 56, 133-149.

Taylor, C.D., Doherty, K.W., 1990. Submersible incubation device (SID), autonomous instrumentation for the in situ measurement of primary and other microbial rate processes. Deep-Sea Research Part A 37, 343-358.

Thompson, R.O.R.Y, 1979. Coherence significance levels. Journal of Atmospheric Sciences 36, 2020-2021.

Warren, B.A., 1972, Insensitivity of subtropical mode water characteristics to meteorological fluctuations. Deep-Sea Research 19, 1-19.

Waters K.J., Smith, R.C., Marra, J., 1994. Phytoplankton production in the Sargasso Sea as determined using optical mooring data. Journal of Geophysical Research 99, 18385-18402.

Yoder, J.A., Atkinson, L.P., Bishop, S.S., Blanton, J.O., Lee, T.N., Pietrafesa, L.J., 1985. Phytoplankton dynamics within Gulf Stream intrusions on the southeastern United States continental shelf during summer 1981. Continental Shelf Research 4, 611-635.

FIGURE CAPTIONS:

Figure 1: Time-depth distributions of a) temperature (C) overlaid with the depth of the nitracline (red line), b) salinity (psu) with the mixed layer depth (red line), c) nitrate (μmol kg^{-1}) with the mixed layer depth (red line), and d) in situ primary production (mgC m^{-3} d^{-1}) with the Z_{Ik} isosurface (where $PAR(z,t)$ equals the I_k estimate, black line).

Figure 2: The upper three panels (a-c) provide time-depth distributions for a) chlorophyll *a* concentration determined by HPLC with depth of the 1% PAR isopleth, b) the diffuse attenuation coefficient for downwelling irradiance of 490 nm, $K_d(z,490,t)$, and depth of the 1% PAR isopleth and c) the ratio of $K_d(z,410,t)$ to $K_d(z,490,t)$, an index for non-algal absorption (Siegel and Michaels, 1996), and the mixed layer depth (black line). The bottom panel is the spectral-time distribution of the remote-sensing reflectance (sr^{-1}).

Figure 3: Scattergraphs between a) in situ chlorophyll *a* concentrations, $Chl(0)$, and chlorophyll estimated from observations of $R_{rs}(0^-,\lambda,t)$, b) $\int Chl$ and $Chl(0)$ and c) $Z_{1\%PAR}$ and $Chl(0)$. In a) optical estimates of chlorophyll were determined using the present BBOP $R_{rs}(0^-,\lambda,t)$ observations (open circles) and the entire SeaBAM data set (dots). Data from SeaBAM are included only if the in situ chlorophyll concentration is less than 0.35 mgChl m^{-3}. Correlation coefficients (r^2) between the OC2v2 algorithm and in situ data are 0.605 and 0.636 for the BBOP and SeaBAM data sets respectively. The root mean square difference between the modeled and observed chlorophyll concentrations are 0.23 mg m^{-3} for the BBOP data set and 0.17 mg m^{-3} for the "SeaBAM-lite" data set. In b) the solid line is the power law fit from the BBOP data, the long dashed line are the Morel and Berthon (1989) power law fit, and the dash-dot line is the BBOP linear fit. In c) the solid line is again the BBOP power law fit and the BBOP linear fit is the dash-dot. Also shown are the Morel (1988) power law fit (long dash line), Smith and Baker (1978) (short-dash line) and Balch et al. (1992) (dotted line). Statistical results for b) and c) may be found in Tables 2a and 2b.

Figure 4: Fit parameters for the Gaussian chlorophyll profile ($Chl_{Gauss}(z,t)$, Equation 3) for a) $C_b(t)$, b) $C_{max}(t)$, c) $\zeta_{max}(t)$ and d) $\Delta\zeta(t)$ as a function of the surface chlorophyll *a*

concentration, Chl(0). Best fit lines for each parameter are shown as the solid lines (see Table 3 for their function forms). Also shown are the results of the Morel and Berthon (1989) global parameterization (dashed lines).

Figure 5: Time series of a) incident PAR flux, $PAR(0^+)$, and modeled clear-sky PAR flux, $PAR_{CS}(0^+)$, (both E m^{-2} d^{-1}), b) water column integrated chlorophyll *a* content, $\int Chl$ (mgChl m^{-2}) and primary production, $\int PP$ (mgC m^{-2} d^{-1}), c) photosynthetic utilization index, Ψ(mgC m^2 $mgChl^{-1}$ E^{-1}), and d) light-photosynthesis parameters, P^*_{sat} and I_k (from Equation 6). Vertical integration of the chlorophyll *a* concentration and primary production profiles with respect to depth is performed over the upper 140 m of the water column.

Figure 6: Time series of BATS $\int PP$ time series (dark solid) and the nine empirical bio-optical $\int PP$ models presented in Table 7 (dashed). Also shown in the "ensemble model" (thin solid line with data points).

Figure 7: Scattergraph of the BF87 $\int PP$ data set and its hindcast model results. The insert shows a random sampling of the BF97 matching the BATS chlorophyll observations (see text). Values of r^2 are 56% for the global data set and 17% for a mean of 100 realizations of the "BF97-lite" sampling experiment. Normalized mean biases are 4% for the global hindcast and –38% for the mean of 100 realizations of the low chlorophyll sampling experiment. Means and variances for the BF97 data set are 881 and 838 mgC m^{-2} d^{-1}, respectively.

Figure 8: Spectral coherence between the observed ∫PP time series and the nine models presented in Table 7 (solid). Coherence estimates are shown for frequencies between 0.002 and 0.024 cycles per day (cpd) which correspond to periods of 500 to 42 days. Estimates of spectral coherence are calculated by linear interpolating the observed and modeled time series onto a regular time base (Δt = 20 days) and calculating discrete Fourier transforms over 25 element, linearly detrended, 80% overlapping windows (Bendat and Piersol, 1986; Emery and Thomson, 1997). A Hanning window is used to reduce spectral leakage. The dotted lines are determinations of a sine wave with periods

of 300 and 400 days superimposed on the BATS sampling schedule with random Gaussian noise equal to the signal variance. Also shown are the 90 and 95% confidence intervals for the coherence estimates (Thompson, 1979).

TABLES:

Table 1: Summary of BBOP Radiometer Deployments

Year	BATS		BBOP	
	Number PP(z) Profiles	Number Chl(z) Profiles	Number Optical Casts	Average number BBOP casts per production day
1992	15	16	506	23
1993	14	15	398	17
1994	14	14	397	18
1995	13	13	389	20
1996	14	18	243	16
1997	13	13	394	22
Average	13.8	14.8	387.8	19.3

Table 2a – Prediction of Chl from Chl(0)

Parameterization	Chl = f(Chl(0))	r^2 (%)	NMB (%)	RMSD (mg m^{-2})
MB89 power law	38.0 $Chl(0)^{0.425}$	52	-39	11.5
BBOP power law	32.4 $Chl(0)^{0.422}$	51	6	6.1
BBOP linear law	74.5 Chl(0) + 15.4	55	0	5.8
MB89 Gaussian	Table 3	55	-11	6.4
BBOP Gaussian	Table 3	55	5	5.9

Estimates of Chl are integrated to 140 m and 82 profiles are used.

Table 2b - Predicting $Z_{1\%PAR}$ from Chl(0)

Parameterization	$Z_{1\%PAR}$ = f(Chl(0))	r^2 (%)	NMB (%)	RMSD (m)
Morel (1988)	38.0 $Chl(0)^{-0.428}$	30	31	44
Balch et al. (1992)	4.6 (6.9 - 6.5 $\log_{10}$(Chl(0)))	32	-28	28
Smith Baker (1978)	4.6 (8.78 - 7.51 $\log_{10}$(Chl(0)))	32	-13	17
BBOP linear	-79.4 Chl(0) + 99.3	30	0	10
BBOP power	70.6 $Chl(0)^{-0.098}$	31	1	10

Table 3 - Gaussian Chlorophyll Profile Parameterizations

parameter	function of Chl(0) (=Chl)	r^2 (%)	NMB (%)
C_b			
BBOP	-0.096*Chl + 0.306	2	0
MB89	0.768 + 0.087*Chl - 0.179*Chl^2 - 0.025*Chl^3	1	-4
C_{max}			
BBOP	-2.186*Chl - 0.440	30	0
MB89	0.299 - 0.289*Chl + 0.579*Chl^2	28	-28
ζ_{max}			
BBOP	-0.459*Chl + 0.414	32	0
MB89	0.600 - 0.640*Chl + 0.021*Chl^2 + 0.115*Chl^3	44	22
$\Delta\zeta$			
BBOP	-0.044*Chl + 0.251 (if Chl $\leq$ 0.1) 1.740*Chl + 2.200 (if Chl > 0.1)	48	0
MB89	0.710 + 0.159*Chl + 0.021*Chl^2	28	255

Table 4 - Chlorophyll Profile Hindcasts (N=655)

Model	r^2 (%)	NMB (%)
BBOP Gaussian	49	-5
Morel & Berthon (1989)	39	2
BBOP Uniform Profile	20	-9

Table 5 - PAR(z,t) and TR(z,t) Modeling (N=650)

Model	PAR(z,t)		TR(z,t)	
	r^2 (%)	NMB (%)	r^2 (%)	NMB (%)
BBOP linear	94	0	97	-2
BBOP power	93	0	97	-2
Morel (1988)	90	22	94	18
Smith & Baker (1978)	94	-8	98	-10
Mean $Z_{1\%}$	93	-2	97	-2

Table 6 Ensemble Mean Determinations

For most determinations, N = 82 (except when P^*_{sat} and I_k are calculated; N = 75).

Quantity	Units	Mean	Stan. Dev.
$PAR(0^+)$	$E\ m^{-2}\ d^{-1}$	31.7	12.5
$PAR(0^+)_{CS}$	$E\ m^{-2}\ d^{-1}$	45.4	13.2
$PAR(0^+)/PAR(0^+)_{CS}$	%	71	20
$Z_{1\%PAR}$	m	91	13
$\int Chl$	$mgChl\ m^{-2}$	23.3	8.7
$\int PP$	$mgC\ m^{-2}\ d^{-1}$	457	231
Ψ	$mgC\ m^2\ mgChl^{-1}\ d^{-1}$	0.751	0.489
P^*_{sat}	$mgC\ mgChl^{-1}\ d^{-1}$	75.6	43.1
I_k	$E\ m^{-2}\ d^{-1}$	5.42	4.47
$I_k/PAR(0^+)$	%	17.8	12.8
Z_{Ik}	m	36.6	14.7
$\int PP(PAR(z) > I_k) / \int PP$	%	48	18

Table 7: Predictions of ∫PP using Global Models

Model	Mean ($mgC\ m^{-2}\ d^{-1}$)	Standard Deviation ($mgC\ m^{-2}\ d^{-1}$)	r^2 (%)	NMB (%)
Observations	457	231	-	-
Ψ based approach				
$<\Psi>$	540	286	27	18
$\Psi = f(Chl)$	481	165	35	6
Ryther & Yentsch (1957)	248	153	34	-46
Behrenfeld & Falkowski (1997a)				
$P^*_{sat} = f(SST)$	369	265	20	-20
P^*_{sat} observed	156	103	73	-66
Sathyendranath & Platt (1985)				
uniform Chl(z)	226	185	19	-50
Gaussian Chl(z)	216	129	22	-53
Waters & Bidigare tuned to BATS	575	141	41	26
Antoine & Morel (1996)				
uniform Chl(z)	497	244	22	18
stratified Chl(z)	347	196	27	-20
"Ensemble Model"	406	157	39	11

Table 8 - P vs. I Modeling

	PP(z,t)		∫PP(t)	
	r^2 (%)	NMB (%)	r^2 (%)	NMB (%)
PAR(z,t) + Chl(z,t)				
$I_k(t)$ & $P^*_{sat}(t)$	82	-1	80	-1
$\langle I_k \rangle$ & $\langle P^*_{sat} \rangle$	53	0	27	-3
$\langle I_k \rangle$ & $P^*_{sat}(t)$	75	-11	65	-13
$I_k(t)$ & $\langle P^*_{sat} \rangle$	53	17	19	16
monthly mean	60	0	31	-3
modeled as f(Chl)	59	-7	28	-8
PAR(z,t) + Chl_{Uni}(z,t)				
$I_k(t)$ & $P^*_{sat}(t)$	50	42	33	35
$\langle I_k \rangle$ & $\langle P^*_{sat} \rangle$	43	37	9	28
$\langle I_k \rangle$ & $P^*_{sat}(t)$	41	33	17	25
$I_k(t)$ & $\langle P^*_{sat} \rangle$	49	52	11	45
PAR(z,t) + Chl_{Gauss}(z,t)				
$I_k(t)$ & $P^*_{sat}(t)$	76	-10	70	-10
$\langle I_k \rangle$ & $\langle P^*_{sat} \rangle$	50	-10	21	-13
$\langle I_k \rangle$ & $P^*_{sat}(t)$	76	-20	63	-22
$I_k(t)$ & $\langle P^*_{sat} \rangle$	48	6	16	6
PAR_{mod}(z,t) + Chl(z,t)				
$I_k(t)$ & $P^*_{sat}(t)$	75	0	80	0
$\langle I_k \rangle$ & $\langle P^*_{sat} \rangle$	56	0	38	-3
$\langle I_k \rangle$ & $P^*_{sat}(t)$	77	-10	76	-12
$I_k(t)$ & $\langle P^*_{sat} \rangle$	53	16	28	15
PAR_{mod}(z,t) + Chl_{Uni}(z,t)				
$I_k(t)$ & $P^*_{sat}(t)$	51	41	41	34
$\langle I_k \rangle$ & $\langle P^*_{sat} \rangle$	47	36	34	26
$\langle I_k \rangle$ & $P^*_{sat}(t)$	45	32	28	24
$I_k(t)$ & $\langle P^*_{sat} \rangle$	51	49	22	42
PAR_{mod}(z,t) + Chl_{Gauss}(z,t)				
$I_k(t)$ & $P^*_{sat}(t)$	71	-10	75	-10
$\langle I_k \rangle$ & $\langle P^*_{sat} \rangle$	55	-12	35	-15
$\langle I_k \rangle$ & $P^*_{sat}(t)$	78	-21	75	-23
$I_k(t)$ & $\langle P^*_{sat} \rangle$	49	4	25	4
monthly means	59	-12	38	-13
modeled as f(Chl)	53	-17	20	-17

Table 9: Role of Time Scale on Predictions of ∫PP using Global Models

Model	sample r^2 (%)	low-pass r^2 (%)	high-pass r^2 (%)	low-pass variability (%)	high-pass variability (%)
Observed	-	-	-	15	77
Ψ based approach					
<Ψ>	27	42	14	23	69
Ψ = f(Chl)	35	50	15	14	67
Ryther & Yentsch (1957)	34	40	21	25	68
Behrenfeld & Falkowski (1997)	20	26	10	18	69
Sathyendranath & Platt					
uniform Chl(z)	19	39	8	20	68
Gaussian Chl(z)	22	56	10	12	71
Waters & Bidigare tuned to BATS	41	51	26	21	75
Antoine & Morel (1996)					
uniform Chl(z)	22	29	13	29	66
stratified Chl(z)	27	46	14	31	67

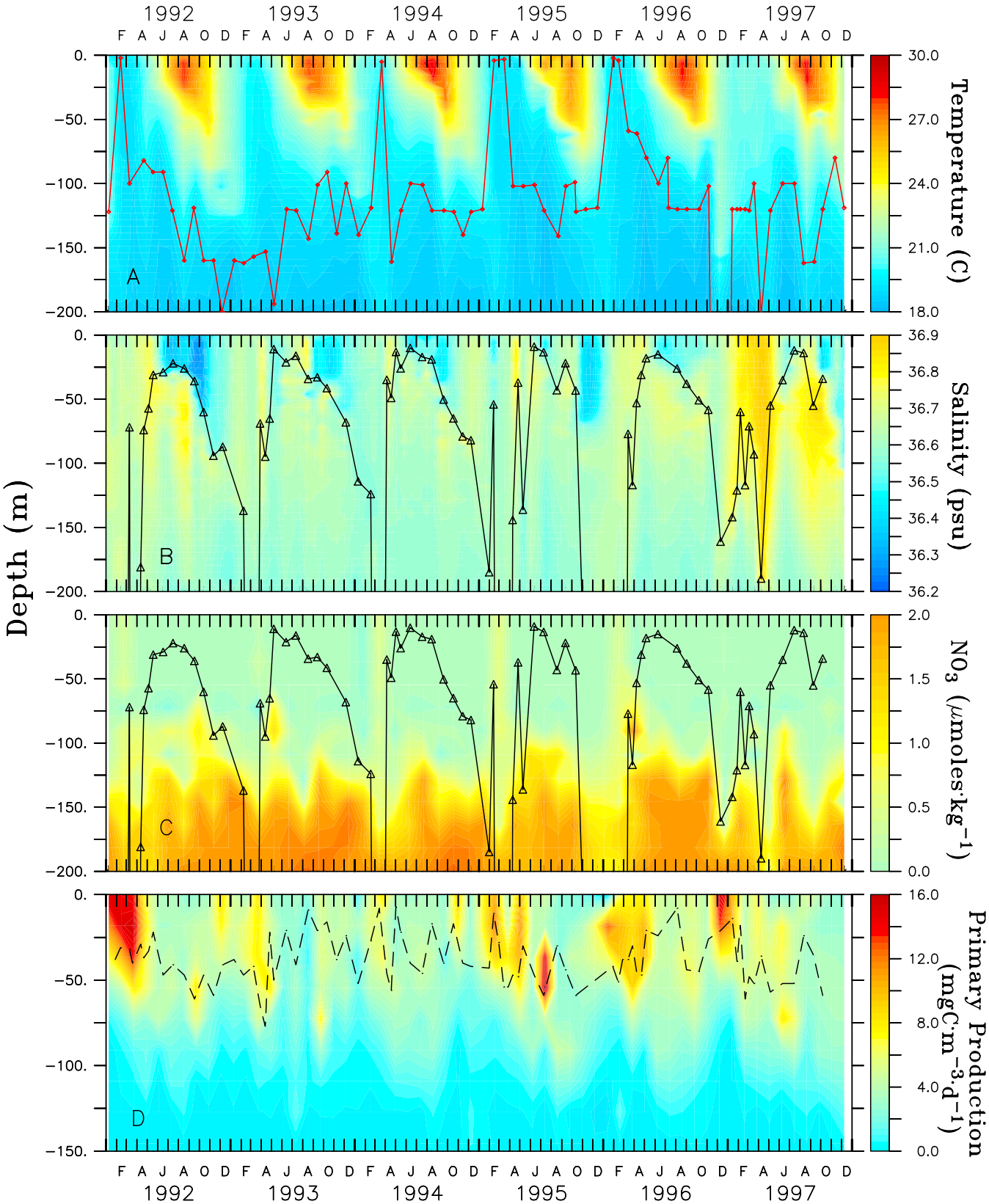

Figure 1 - Siegel et al

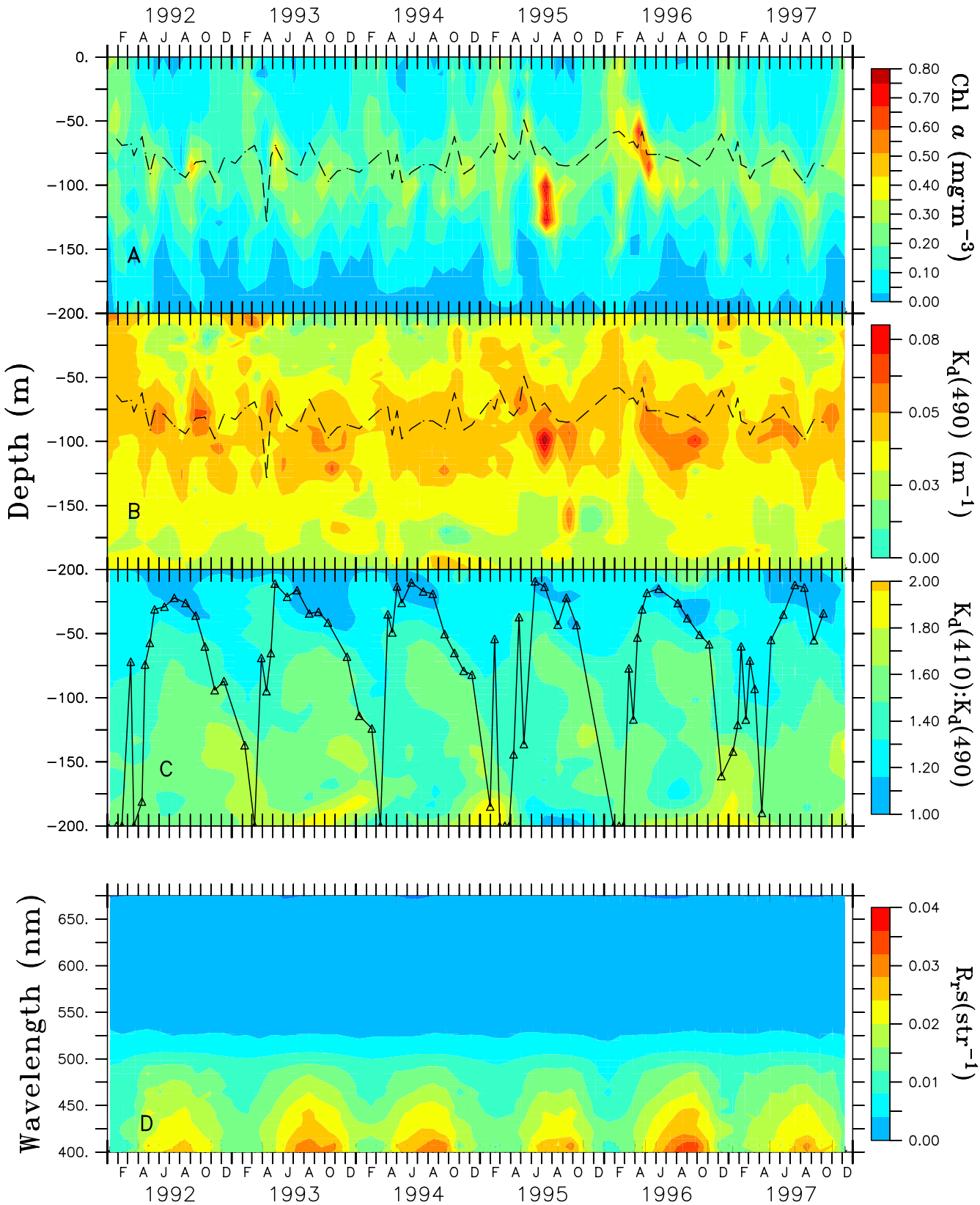

Figure 2 - Siegel et al

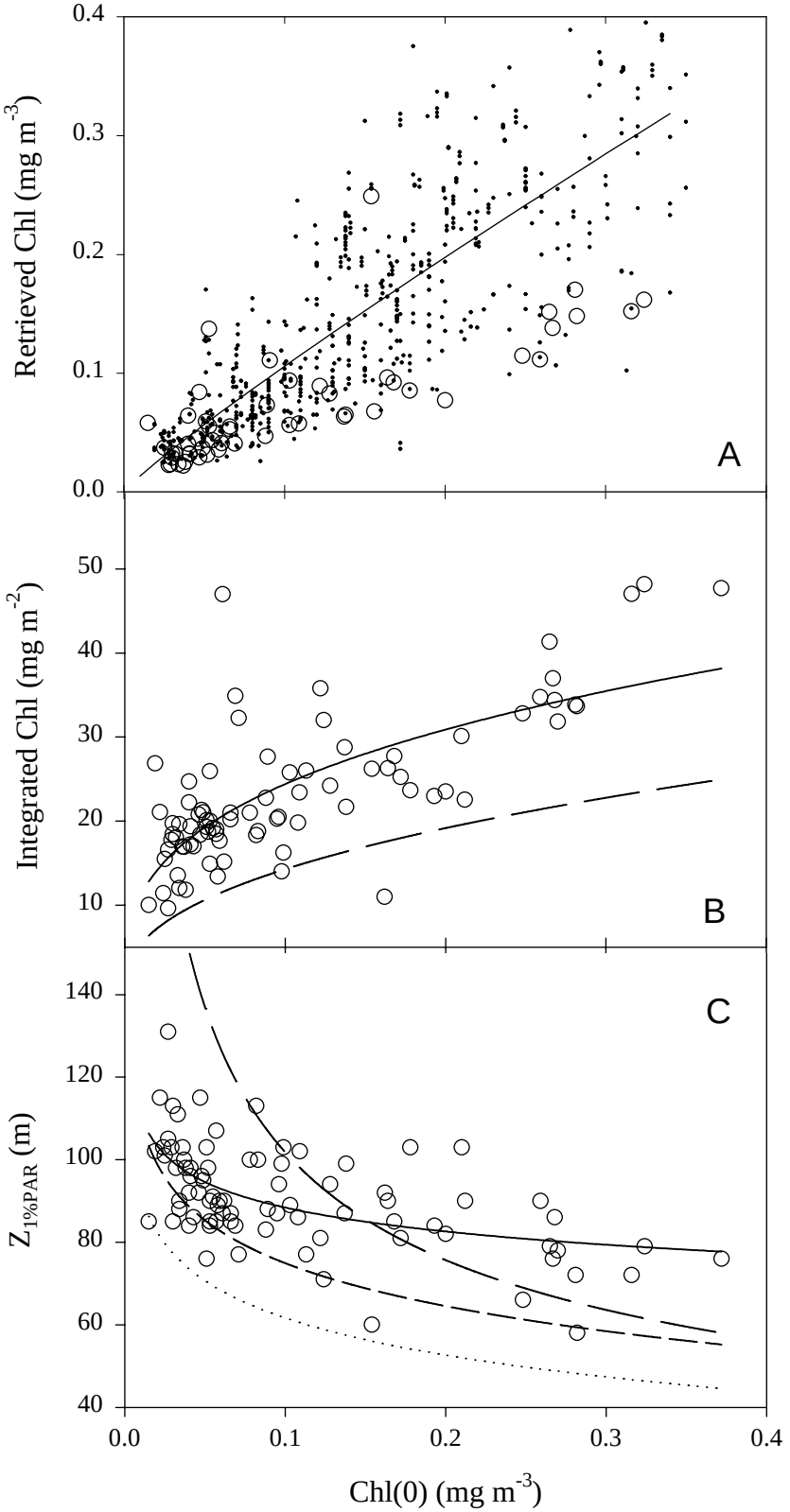

Figure 3 - Siegel et al

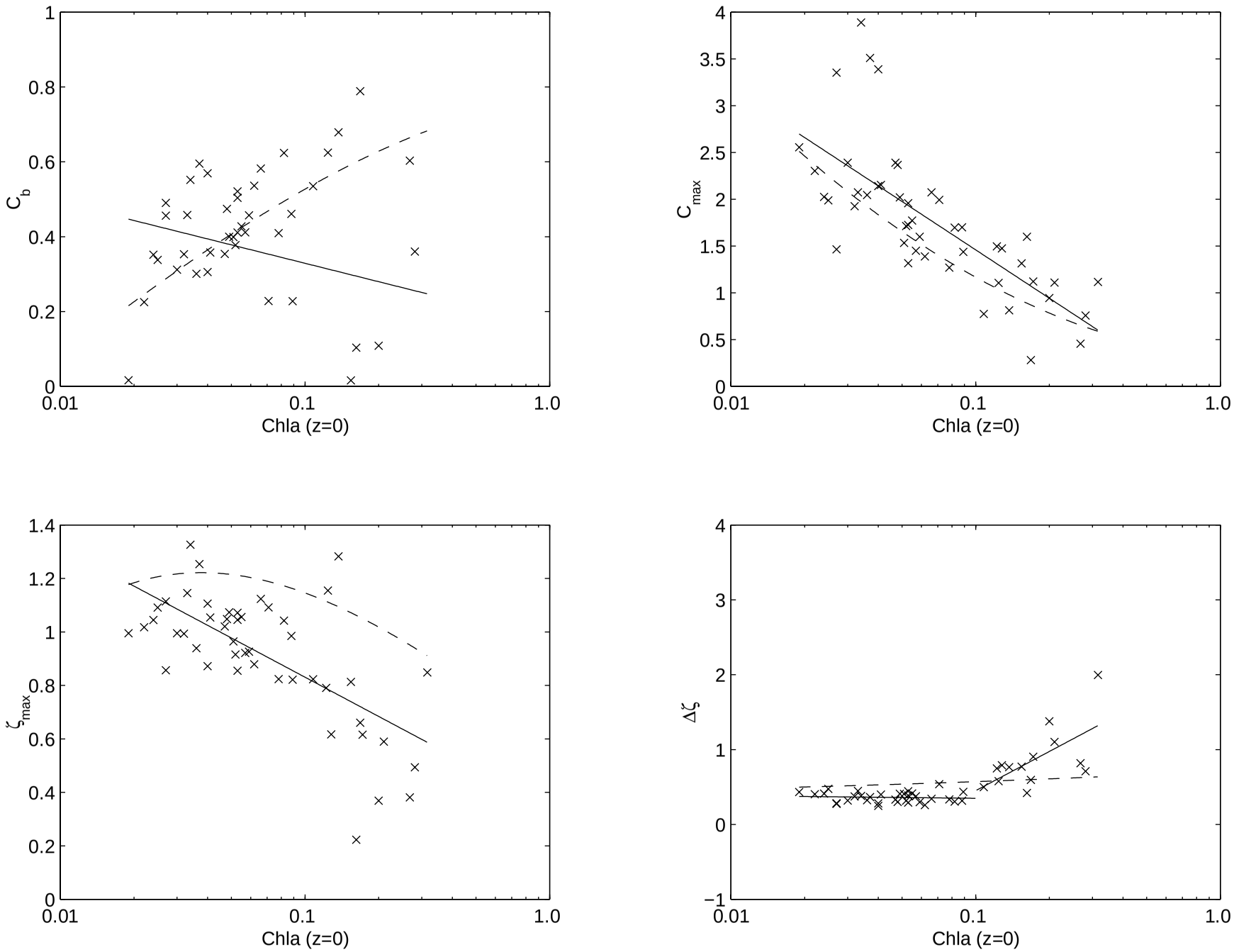

Figure 4 - Siegel

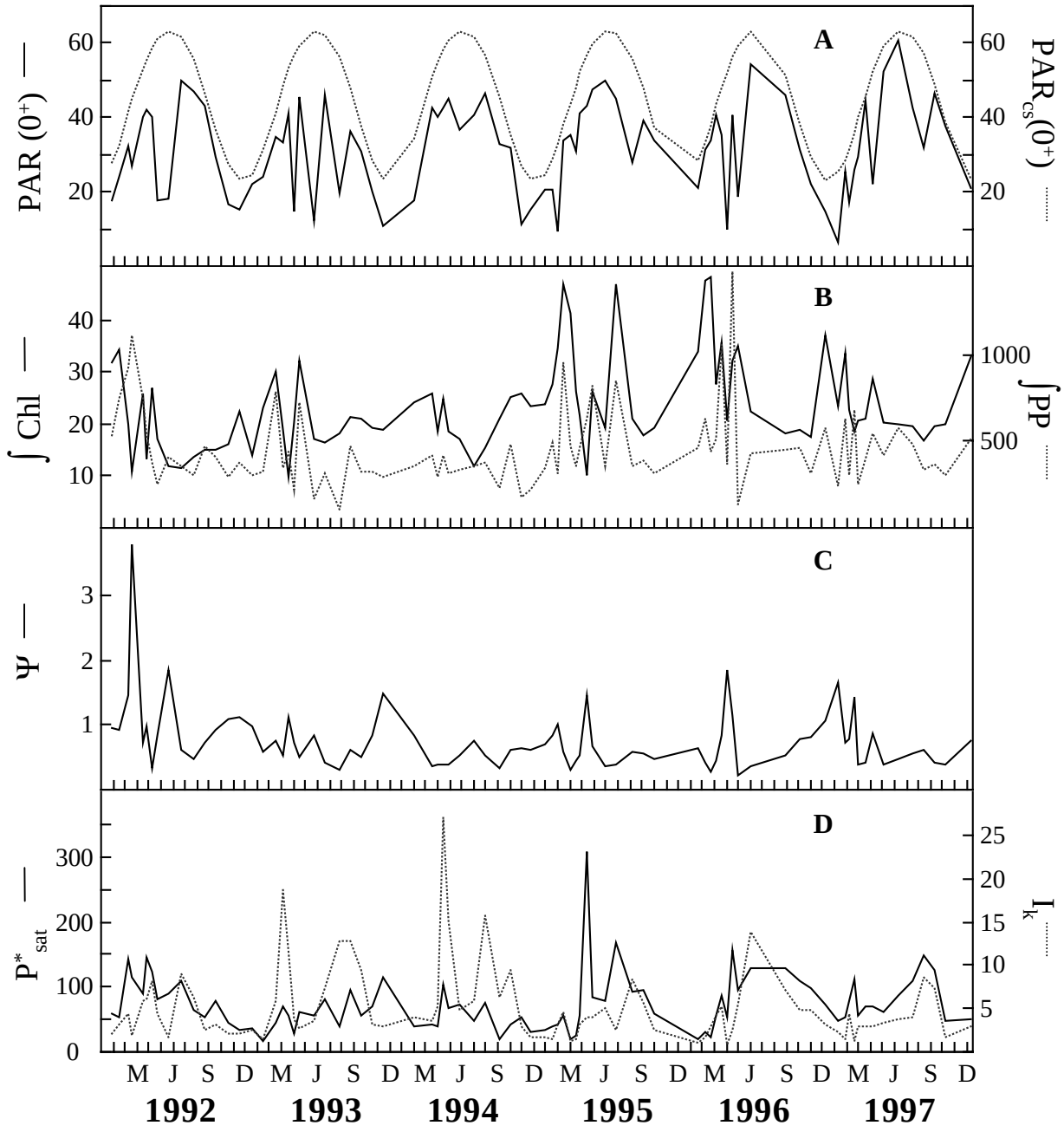

Figure 5 - Siegel et al

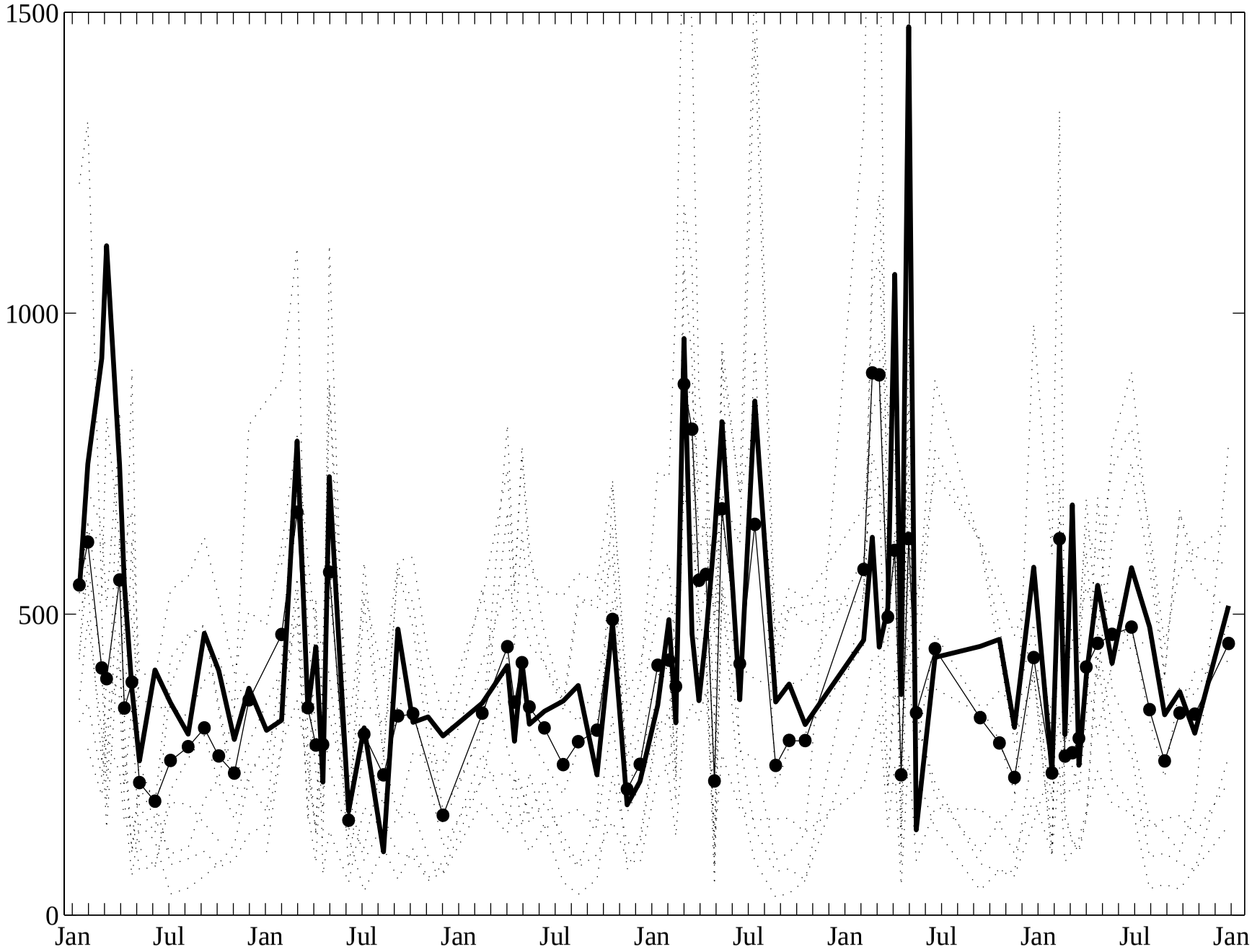

Figure 6 - Siegel

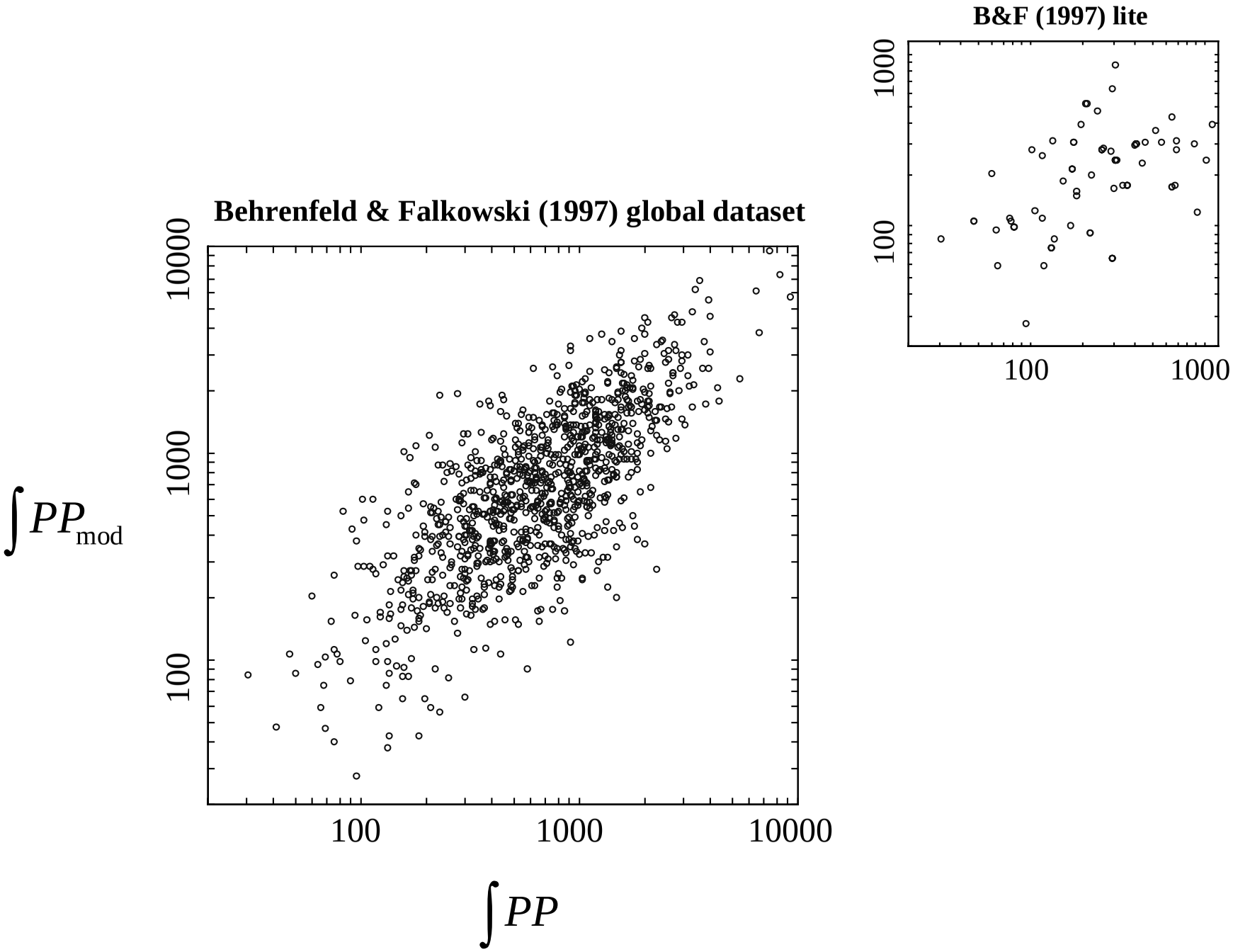

Figure 7 - Siegel et al

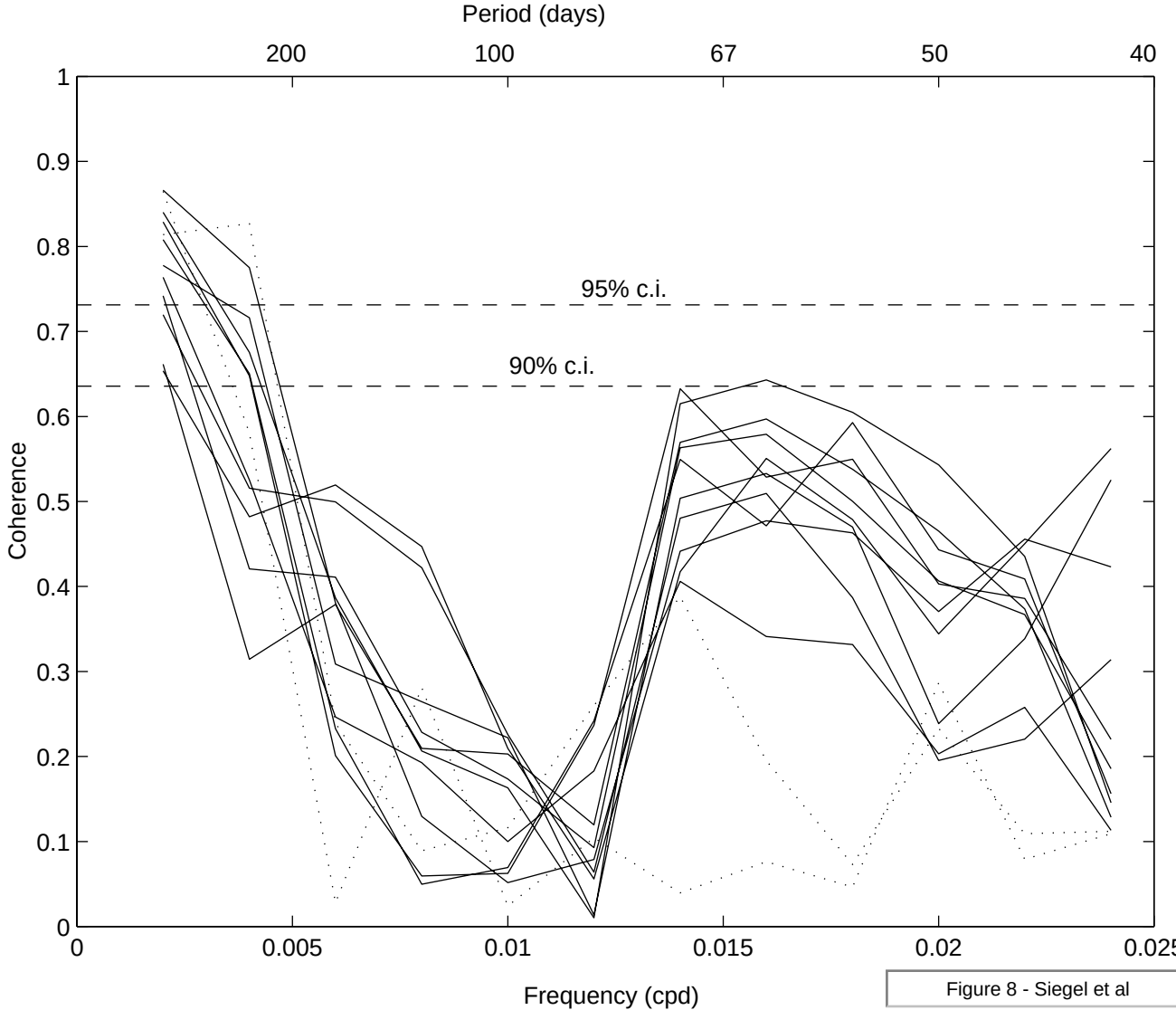

Figure 8 - Siegel et al